Authors' final (accepted) version
Published as: Nucl. Fusion 62, 126032, 2022
https://doi.org/10.1088/1741-4326/ac9006

Staircase Formation by Resonant and Non-resonant Transport of Potential Vorticity

Qinghao Yan[1,2,*] and Patrick H. Diamond[1,3]

[1] *Center for Fusion Sciences, Southwestern Institute of Physics, Chengdu, Sichuan 610041, People's Republic of China*
[2] *Department of Engineering Physics, Tsinghua University, Beijing 100084, People's Republic of China*
[3] *Center for Astrophysics and Space Sciences (CASS) and Department of Physics, University of California San Diego, La Jolla, California 92093, USA*

(Dated: October 29, 2022)

The $E \times B$ staircase is a quasi-periodic pattern of pressure profile corrugations. In this work, we present a new mechanism for $E \times B$ staircase formation, that involves resonant transport verses non-resonant transport. We start from a potential vorticity evolution system and use quasi-linear theory, a model dispersion relation, and a bi-Lorentzian spectrum approximation, to construct the relation between the fluxes and the profiles. With these fluxes, we close the profile evolution equations and the extended turbulence intensity evolution equation, which together constitute a turbulence-profile evolution system. In this system, the Doppler effect from the $E \times B$ mean flow can cause resonance between trapped ion precession motion and the trapped ion mode, which drives a resonant transport contribution to the fluxes. The profiles will be flattened where the resonant transport is switched on. In contrast, for the regions of non-resonant transport, profiles are steeper. A quasi-periodic pattern of profile corrugation (the $E \times B$ staircase) spontaneously emerges in this system, which is the two states mentioned above, arranged as alternating layers in space. The feedback processes during the staircase pattern formation are identified. An estimate of the critical value of the boundary heat flux is obtained, above which staircase formation will be triggered. An estimate scaling of the step size in the staircase pattern is obtained. The resonant turbulent transport is also a mechanism for collisionless saturation of zonal flow. This work is related to internal transport barrier (ITB) formation and suggests some new scenarios, such as an enhanced confined L mode.

I. INTRODUCTION

Drift wave turbulence in confined plasma is now widely realized to be a self-regulating system. Indeed, the now classic "drift wave turbulence" problem has, over time, evolved into a pattern formation problem, with primary focus on understanding secondary structure, such as zonal flows[1, 2] and avalanches[3–5]. Interestingly, these two structures divide the possible states of profiles and transport into two classes, namely shearing and barrier formation for the former; and stronger transport driven by a scale independent distribution of mixing events for the latter. Of course, transport barriers can be viewed as localized regions of particularly strong enhancement of confinement, where profiles steepen sharply, and transport drops to near-neoclassical levels. Recently, awareness and interest in staircases have grown[6–15]. In contrast to single barriers, staircases are *quasi-periodic layered patterns*, where regions of strong transport and profile flattening alternative with "mini-barriers"[9, 13], where profiles steepen. The mini-barriers are frequently (but not always) accompanied by zonal flow shear layers. The sequence of alternating profile flattening regions and mini-barriers loosely resembles a staircase, and is so named. It should be noted that staircases are a particular case of the general phenomenon of "layering", which appears in, and is of quite general interest to, a wide variety of fields, such as double diffusive convection[16–18], oceanic mixing[19, 20], arctic ice structures[21, 22], etc.

The central question of layering and staircase formation is that of *scale selection*. Indeed, the physics of zonal flow scale is still unclear[10, 23, 24]. Staircases result form inhomogeneous mixing process (as in potential vorticity homogenization), and are frequently linked to anti-diffusion (as for the Cahn-Hilliard equation) [25–27] and self-sharpening of shears(as in jet formation)[28, 29]. These processes play out in a variety of ways, in a wide variety of models. However, one particular approach - that of bi-stable mixing, developed by Balmforth et. al [30] (BLY) is of particular interest and relevance to staircase formation in drift wave turbulence and transport. The BLY theory is cast in a $K - \varepsilon$ framework and aims to calculate profiles and turbulence intensity, utilizing ideas from mixing length theory. The simple-but-novel feature of BLY is the interplay between mixing length scales, one of which is linked to the scale of excitation, and one of which is emergent and dependent upon the local gradient of the transported quantity. Examples of emergent scales are the Ozmidov scale[31] in mixing and the Rhines scale[32] in beta plane turbulence. Both these

* qinghaoyan@outlook.com

scales are defined by dynamic balance. Of course, it is the interplay between these two scales of mixing which allows the modelling of a staircase pattern, consisting of layers of two characteristic regions. In the BLY model, the transport flux is bistable and transport bifurcations occur at the interfaces between steps(regions of flattening) and jumps(mini-barriers). The interplay of the two scales naturally realizes the concept of "inhomogeneous mixing". BLY-type models have been very successful in describing turbulent mixing in stratified fluids and have recently been extended to drift wave turbulence[9, 33].

Virtually all approaches to the layering problems have been in the context of hydrodynamics models and problems. Yet confined plasms are collisionless, the turbulence is kinetic and mixing can occur via resonant wave-particle interactions. Particles orbit stochasticity is fundaments to mixing in such plasmas. Hence, the layering should reflect orbit dynamics. Staircases have been observed in gyro-kinetic simulations[7, 8, 11, 13]. These considerations naturally open the door to an interesting alternative to the BLY mechanism, namely one in which *the two states of mixing are those due to resonant and non-resonant transport,* respectively.

In this paper, we present a novel approach to staircase formation in a turbulent, collisionless plasma, due to the interplay of resonant and non-resonant diffusion. Of course, $D_{\rm res} \neq D_{\rm non-res}$, so the two processes mix at different rates. We develop the theory in the context of the Darmet model[34–36] of trapped-ion drift wave and ion temperature gradient (ITG) turbulence. The Darmet model is perhaps the very simplest drift wave-type model which manifests resonant transport (due to the magnetic precession drifts), zonal flows, resonant transport of vorticity (due to wave resonance with $E\times B$ flows) as well as the usual hydrodynamic transport mechanisms familiar in drift wave turbulence. It is simple but representative. A key element of the staircase formation story is that the wave-particle resonance is set by the difference between ω and $\omega_{Di}+\omega_Z$, where ω is the wave frequency, ω_{Di} is the precession frequency and ω_Z is the zonal or $E\times B$ frequency. Should ω_Z vary, due to the spatial structure of the zonal flow defined by the mean vorticity balance. $\omega-\omega_{Di}-\omega_Z$ will then vary between zero (i.e. resonant) and finite (i.e. non-resonant) limit. Consequently, heat transport then also varies between resonant and non-resonant states, thus allowing layering. In a sense, one may think of this theory as a parallel to the two scale approach of BLY, with instead two diffusivities, resonant and non-resonant, obtained for the specified case of the Darmet model. And of course, stripe formation - analogous to layering - is a familiar outcome of Turing pattern formation, which involve two unequal diffusivities[37]. Needless to say, the ratio $D_{\rm res}/D_{\rm non-res}$ is crucial to the model we present here.

The theory consists of coupled equations for heat transport, zonal vorticity and potential enstrophy (which gives the fluctuation intensity). Transport coefficients are derived by quasilinear theory. Since transport is driven by $|\tilde{\phi}|^2$ which is derived from potential enstrophy by a Green's function and which is thus spatially smooth, we focus on the temperature and vorticity equations as the essential staircase model. These are solved for (fixed) flux boundary conditions. Two types of regions emerge form the solution:

1. Type I $\rightarrow$ peaked profile layers, manifesting non-resonant transport

2. Type II $\rightarrow$ flat profile spots, manifesting resonant transport

Together, these two define the staircase. The step scale is $\propto \delta_b$, the banana orbit width. The conditions for staircase formation are derived. The role of proximity to marginal stability is discussed at length.

The remainder of this paper is organized as follows. Section II presents and discusses the Darmet model as a potential vorticity (PV) conserving system. The transport fluxes, both resonant and non-resonant, are calculated in section III. The flux model is simplified in section IV, which is where the important approximations are discussed. Section V presents the analysis of staircase formation, and gives the key results. The trigger criterion for staircase onset is derived. Key feedback loops are traced. Section VI gives a discussion and conclusions.

II. A POTENTIAL VORTICITY CONSERVING SYSTEM

For the study of low-frequency ($\omega < \omega_b < \Omega_i$) turbulence in a tokamak, the gyro phase and bounce phase in the kinetic distribution function can be averaged. This leads to a double phase averaged distribution function $\bar{f}$, which is three dimensional in the phase space with dependence on ψ, α, E. Here ψ and α are the radial and angle coordinates, and E is the energy or velocity coordinate. $\bar{f}$ is determined by the kinetic equation[34–36]:

$$\partial_t \bar{f} + \Omega_D E \partial_\alpha \bar{f} - [J_0\phi, \bar{f}] = 0 \tag{1}$$

where $[F,G] = \partial_\alpha F \partial_\psi G - \partial_\psi F \partial_\alpha G$, and J_0 is a gyro- and bounce-averaging operator. Here $\Omega_D E$ is the precession frequency of trapped particles, and Ω_D is assumed to be constant. Because the length scales after phase averaging are the banana width and gyro-radius (both of which exceed the Debye length), the Poisson equation is replaced by the quasi-neutrality constraint $n_i = n_e$.

Then a decomposition to the phase-averaged distribution function $\bar{f}$ is possible:

$$\bar{f} = \langle f \rangle - \langle f \rangle \frac{q_{i,e}\phi}{T_{i,e}} + h_{i,e} \tag{2}$$

where $\langle f \rangle$ is the mean distribution and varies only in ψ, $-\langle f \rangle q_{i,e}\phi/T_{i,e}$ is the adiabatic response part of $\tilde{f}$, and $h_{i,e}$ is the non-adiabatic part. Here we assumed

$|q_i\phi/T_{i,e}| \ll 1$. We also need to recognize the zonal portion $\phi_Z \equiv \langle\phi\rangle_\alpha$, and the fluctuating portion $\tilde{\phi}$, of ϕ. The adiabatic response portion in Eq.(2) should only be specified for the fluctuation portion, i.e. in the simple form: $\widetilde{n}_{i,e}/n_0 = -q_{i,e}(\phi - \langle\phi\rangle_\alpha)/T_{i,e}$. Substituting the the decomposition of the distribution function into the quasi-neutrality condition, we have,

$$\begin{aligned}&\frac{2}{n_0\sqrt{\pi}}\int_0^\infty J_0\left[-\frac{q}{T_i}(\phi-\phi_Z)\langle f_i\rangle + h_i\right]\sqrt{E}\mathrm{d}E + \overline{\Delta}_i\frac{q_i\phi}{T_i}\\ &= \frac{2}{n_0\sqrt{\pi}}\int_0^\infty J_0\left[\frac{q}{T_e}(\phi-\phi_Z)\langle f_e\rangle + h_e\right]\sqrt{E}\mathrm{d}E - \overline{\Delta}_e\frac{q_i\phi}{T_e}\end{aligned} \tag{3}$$

$\overline{\Delta}_s = \rho_{0s}^2\partial_\alpha^2 + \delta_{bs}^2\partial_\psi^2$ accounts for the polarization - caused by the density difference between the double-averaged centers and actual particles. We apply the normalization below:

$$\hat{E} = \frac{E}{T_0}, \quad \hat{t} = \omega_0 t, \quad \hat{\psi} = \frac{\psi}{L_\psi}, \quad \hat{\phi} = \frac{\phi}{L_\psi\omega_0}, \quad \hat{\Omega}_D = \frac{\Omega_D T_0}{\omega_0}$$

where ω_0 is the typical precession frequency, $L_\psi \equiv aR_0B_\theta$ is the box size in magnetic flux unit, $\Omega_D T_0$ has the same unit of ω_0. Such normalization will not change the essential form of Eq.(1) and Eq.(3), but change q_i/T_i to $\omega_0 L_\psi q_i/T_i$. So we will neglect the notation " $\hat{}$ " in the following derivations.

Eq.(3) could be included in Eq.(5), a kinetic quasi-neutrality equation, whose R.H.S. is determined only by the non-adiabatic particle distribution functions $h_{i,e}$. Meanwhile, the non-adiabatic distribution function h_i satisfies the kinetic equation Eq.(4):

$$\begin{aligned}&\partial_t h_i + \Omega_D E\partial_\alpha h_i - \left[\bar{\phi}, -C_i(\phi-\phi_Z)\langle f_i\rangle + h_i\right]\\ &\quad = \partial_t\left(C_i(\phi-\phi_Z)\langle f_i\rangle\right) + \partial_\alpha(\overline{\phi-\phi_Z})\partial_\psi\langle f_i\rangle\end{aligned} \tag{4}$$

$$\begin{aligned}&C_{ad}\left(\phi-\phi_Z\right) - C_i\overline{\Delta}_{i+e}\phi\\ &\quad = \frac{2}{n_0\sqrt{\pi}}\left(\int_0^\infty J_0 h_i\sqrt{E}\mathrm{d}E - \int_0^\infty J_0 h_e\sqrt{E}\mathrm{d}E\right)\\ &\quad = \widetilde{n}_{\mathrm{nonad},i} - \widetilde{n}_{\mathrm{nonad},e}\end{aligned} \tag{5}$$

Here $C_i = \omega_0 L_\psi q_i/T_i$, $C_{ad} = C_i(1+\tau)/\sqrt{2\varepsilon_0}$, $\tau = T_i/T_e$, $\overline{\Delta}_{i+e} = \overline{\Delta}_i + \tau\overline{\Delta}_e$. $(\overline{\phi-\phi_Z})$ represents the double-phase-averaged potential. $\varepsilon_0 = a/R$ is the inverse aspect ratio, and $\sqrt{2\varepsilon_0}$ is the fraction of trapped particles. In the kinetic quasi-neutrality Eq.(5), we can assume adiabatic electrons, i.e. $h_e = 0$, and neglect the $\overline{\Delta}_e$ term. Eq.(4)-(5) are called the Darmet model, and its variants are used in reduced gyro-kinetic simulations of trapped ion mode (TIM) and interchange-like turbulence[34–36, 38, 39]. The Darmet model can be viewed as the minimal kinetic system for drift wave turbulence, which contains wave-particle resonance effects. The fact that the TERESA code (based on the Darmet model) can produce a staircase profile [40] is evidence that the Darmet model contains the physics for staircase formation.

As we first pointed out in Ref.[41], Eq.(4)-(5) can be written as a potential vorticity conserving system. Below, we will show how.

First, taking the derivative of Eq.(5) with respect to time, the non-adiabatic contribution in the R.H.S. becomes $\partial_t h_i$. Using Eq.(4) to eliminate $\partial_t h_i$, and doing the energy integral, yields,

$$\begin{aligned}&\partial_t\left[C_e(\phi-\phi_Z) - C_i\overline{\Delta}_i\phi\right] =\\ &\quad -\frac{3}{2}\frac{\Omega_D}{T_0}\partial_\alpha\widetilde{T}_i + \left[\phi, -\frac{C_i}{\sqrt{2\varepsilon_0}}(\phi-\phi_Z) + \frac{\widetilde{n}_i}{n_0}\right]\\ &\quad -\frac{1}{\sqrt{2\varepsilon_0}}\widetilde{V}(\psi)\partial_\psi\ln\langle n_i\rangle\end{aligned} \tag{6}$$

where $C_e = C_i\tau/\sqrt{2\varepsilon_0}$, and we simply take $J_0\phi = \bar{\phi} = \phi$. When doing the integral of $\langle f_i\rangle$, we encounter the factor $1/\sqrt{2\varepsilon_0}$, because $\langle f_i\rangle$ is the distribution function of all particles, including both passing and trapped. Remember that $\phi_Z \equiv \langle\phi\rangle_\alpha$, so we write $\phi = \tilde{\phi} + \phi_Z$, where $\tilde{\phi}$ is due to $n \neq 0$ trapped ion modes. After replacing $\tilde{n}_i$ with Eq.(5), we can separate the results into two equations according to symmetry[42–44], as below. The subscript i in $\overline{\Delta}_i$ is neglected.

$$\begin{aligned}&\left(\frac{\partial}{\partial t} + \widetilde{\mathbf{V}}\cdot\nabla + \mathbf{\Omega}_Z\cdot\nabla\right)\left(C_i\overline{\Delta}\tilde{\phi}\right) = \frac{3}{2}\frac{\Omega_D}{T_0}\partial_\alpha\widetilde{T}_i\\ &\quad -iC_e(\omega - \omega_Z + \frac{\omega^i_{*n}}{\tau})\tilde{\phi} - C_i\widetilde{V}_\psi\partial_\psi(\overline{\Delta}\phi_Z)\end{aligned} \tag{7}$$

$$\begin{aligned}\frac{\partial}{\partial t}\left(C_i\overline{\Delta}\phi_Z\right) &= C_i\langle\nabla\tilde{\phi}\times\hat{z}\cdot(\nabla\overline{\Delta}\tilde{\phi})\rangle_\alpha\\ &\equiv -C_i\delta_{b0}^2\partial_\psi^2\left\langle\tilde{V}_\psi\tilde{V}_\alpha\right\rangle_\alpha\end{aligned} \tag{8}$$

where $\widetilde{\mathbf{V}} = -\nabla\tilde{\phi}\times\hat{z}$, $\mathbf{\Omega}_Z = -\nabla\phi_Z\times\hat{z} = \partial_\psi\phi_Z\hat{\mathbf{e}}_\alpha$. The Doppler shift effect terms are $\omega^i_{*n} = \frac{k_\alpha c}{C_i}\partial_\psi\ln\langle n_i\rangle$, $\omega^i_{*T} = \frac{k_\alpha c}{C_i}\partial_\psi\ln\langle T_i\rangle$, $\omega_Z = k_\alpha\partial_\psi\phi_Z$. The magnetic field is included in $\mathrm{d}\psi = -B_\theta R_0\mathrm{d}r$, where r is the minor radius and R_0 is the major radius. It's obvious that Eq.(7)-(8) are the evolution equations for vorticity and "zonal vorticity" (or flow shear). In Eq.(7), the second term on the R.H.S can be combined with the L.H.S., yielding an evolution equation for $\tilde{\phi} - \overline{\Delta}\tilde{\phi}$, which has a structure similar to the Hasegawa-Mima equation [45]. Eq.(8) shows that zonal vorticity evolves according to Reynolds force, as expected. Clearly, Eq.(7) and (8) are not a closed system. We need to determine how the fluctuating temperature $\widetilde{T}_i$ (on the R.H.S of eq.(7)) evolves.

An evolution equation for $\widetilde{T}_i$ is required to close the system. We can substitute the full $\bar{f}_i$ and ϕ into the kinetic Eq.(1), and then obtain the temperature evolution by taking the energy moment, i.e. $\frac{2}{3}\frac{2}{n_0\sqrt{\pi}}\int_0^\infty ...E\sqrt{E}\mathrm{d}E$. Then separating the result according to symmetry, we

have:

$$\begin{aligned}\sqrt{2\varepsilon_0}\left(\partial_t+\widetilde{\mathbf{V}}\cdot\nabla+\mathbf{\Omega}_Z\cdot\nabla\right)\widetilde{T}_i\\ =-i(\omega-\omega_Z-\omega^i_{*n}-\omega^i_{*T})\langle T_i\rangle C_i\tilde{\phi}\end{aligned}\tag{9}$$

$$\begin{aligned}\frac{\partial}{\partial t}\left(\langle T_i\rangle+\langle T_i\rangle\ln\langle n_i\rangle\right)=\sqrt{2\varepsilon_0}\langle\nabla\tilde{\phi}\times\hat{z}\cdot\nabla\widetilde{T}_i\rangle_\alpha\\ \equiv-\sqrt{2\varepsilon_0}\partial_\psi\langle\widetilde{V}_\psi\widetilde{T}_i\rangle_\alpha\end{aligned}\tag{10}$$

From Eq.(7) to Eq.(10), the system is closed. We will neglect ω^i_{*n} and $\ln\langle n_i\rangle$ by assuming large $L_n\equiv\partial_\psi\ln\langle n\rangle$ due slow variation of mean density. In other words, the mean density gradient is neglected in our model. Notice the similarity between Eq.(7) and Eq.(9), which means they can be written in a simpler form. First, multiply the above equations (9)-(10) by $\tau/(\sqrt{2\varepsilon_0}\langle T_i\rangle)$. Then subtract the two vorticity equations (7)-(8) from equations (9)-(10), respectively. After these steps, we have:

$$\begin{aligned}\frac{\partial}{\partial t}\left(\frac{\tau}{\sqrt{2\varepsilon_0}}\ln\langle T_i\rangle-C_i\overline{\Delta}\phi_Z\right)\\ =\left\langle\nabla\tilde{\phi}\times\hat{z}\cdot\nabla\left(\frac{\tau}{\langle T_i\rangle}\nabla\widetilde{T}_i-C_i\overline{\Delta}\tilde{\phi}\right)\right\rangle_\alpha\end{aligned}\tag{11}$$

$$\begin{aligned}\frac{\mathrm{d}}{\mathrm{d}t}\left(\tau\frac{\widetilde{T}_i}{\langle T_i\rangle}-C_i\overline{\Delta}\tilde{\phi}\right)\\ =-\frac{3}{2}\frac{\Omega_D}{T_0}\partial_\alpha\widetilde{T}_i-\widetilde{\mathbf{V}}\cdot\nabla\left(\frac{\tau}{\sqrt{2\varepsilon_0}}\ln\langle T_i\rangle-C_i\overline{\Delta}\phi_Z\right)\end{aligned}\tag{12}$$

Finally, the two equations above can be written as evolution equations for mean and fluctuating *potential vorticity* (PV).

$$\partial_t\langle q\rangle=\left\langle\nabla\tilde{\phi}\times\hat{z}\cdot\nabla\delta q\right\rangle_\alpha=-\partial_\psi\left\langle\widetilde{V}_\psi\delta q\right\rangle_\alpha\tag{13}$$

$$\frac{\mathrm{d}}{\mathrm{d}t}\delta q=-\frac{3}{2}\frac{\Omega_D}{T_0}\partial_\alpha\widetilde{T}_i-\widetilde{\mathbf{V}}\cdot\nabla\langle q\rangle\tag{14}$$

where the total potential vorticity $\langle q\rangle+\delta q$ is defined as,

$$\langle q\rangle=\frac{\tau}{\sqrt{2\varepsilon_0}}\ln\langle T_i\rangle-C_i\overline{\Delta}\phi_Z\tag{15}$$

$$\delta q=\tau\frac{\widetilde{T}_i}{\langle T_i\rangle}-C_i\overline{\Delta}\tilde{\phi}\tag{16}$$

and

$$\frac{\mathrm{d}}{\mathrm{d}t}=\frac{\partial}{\partial t}+\widetilde{\mathbf{V}}\cdot\nabla+\mathbf{\Omega}_Z\cdot\nabla$$

Eq.(13)-(14) are the system for PV we first obtained in Ref.[41], where the total PV is conserved up to the curvature drift. Potential vorticity is the extension of vorticity. The PV perspective is very powerful for studies of quasi-geostrophic (QG) theory[46–49] and magnetic fusion plasma[45, 50–52]. Since the goal of this paper is to study profile evolution, we study the mean PV evolution Eq.(13), which contains both the mean temperature and the mean vorticity profile contributions. But Eq.(13) is determined by the PV flux on the R.H.S., where PV flux has contributions from both $\widetilde{T}_i$ and $\tilde{\phi}$. Therefore it will connect the PV flux to the heat flux and vorticity flux, which require the knowledge from Eq.(7) and Eq.(9). So even though Eq.(13)-(14) are tidy, they are not very useful for the study of profile evolution. The better way is to use Eq.(7)-(10) instead. All in all, the fact that the full evolution Eq.(7)-(10) is actually a PV-conserving system is indeed interesting.

III. MEAN FLUXES

The ultimate goal of this paper is to study $E\times B$ staircases, i.e. quasi-periodic patterns in $\langle T\rangle$ and ϕ_Z. Through our PV conserving system in the previous section, we know that the mean profile evolution follows the equations below:

$$\frac{\partial}{\partial t}\ln\langle T\rangle=-\sqrt{2\varepsilon_0}\partial_x\langle\widetilde{V}_x\widetilde{T}\rangle_y\tag{17}$$

$$\frac{\partial}{\partial t}\left[\overline{\Delta}\phi_Z\right]=-\partial_x\left\langle\widetilde{V}_x\overline{\Delta}\tilde{\phi}\right\rangle_y\tag{18}$$

where we change the notation into $(\psi,\alpha)\to(x,y)$ for the purpose of simplicity. The evolutions of mean profiles are determined by the fluxes on the R.H.S. A frequently used approach for obtaining fluxes is the quasi-linear (QL) approximation, which approximates the flux by connecting two fluctuation quantities using a (quasi-)linear relation. Since we already included all the evolution of the fluctuating quantities in the PV conserving system Eq.(7)-(10), we can easily obtain the quasi-linear fluxes. Before the derivation, we define some quantities as below:

$$\begin{aligned}\bar{\Omega}_D=\frac{3}{2}\frac{\Omega_D}{C_i},\omega_{*n}=0,\tau=\frac{T_i}{T_e}=1,\widetilde{T}=\frac{\widetilde{T}_i}{\langle T_i\rangle},\\ C_e=\frac{C_i\tau}{\sqrt{2\varepsilon_0}},A=C_e/C_i=\frac{\tau}{\sqrt{2\varepsilon_0}}\end{aligned}$$

The first step to obtain the QL fluxes is applying a Fourier transformation to the fluctuating evolution Eq.(7) and Eq.(9).

For the evolution Eq.(7) related to $\tilde{\phi}$, we note the possibility of writing a conservative equation for fluctuation quantity, $\tilde{U}\equiv A\tilde{\phi}-\overline{\Delta}\tilde{\phi}$. This is similar to the potential vorticity evolution defined by the Hasegawa-Mima equation [45]. Conservation of $\tilde{U}$ is broken by the fluctuating temperature and curvature drift, and zonal potential. With quantities we defined above, Eq.(7) is written as:

$$\begin{aligned}\left(\frac{\partial}{\partial t}+\widetilde{\mathbf{V}}\cdot\nabla+\mathbf{\Omega}_Z\cdot\nabla\right)\overline{\Delta}\tilde{\phi}\\ =\bar{\Omega}_D\partial_y\widetilde{T}-iA(\omega-\omega_E)\tilde{\phi}-\widetilde{V}_x\partial_x\overline{\Delta}\phi_Z\end{aligned}\tag{19}$$

Writing the evolution in terms of $\tilde{U}$, gives:

$$\begin{aligned}\left(\frac{\partial}{\partial t}+\Omega_Z\cdot\nabla\right)\left(A\tilde{\phi}-\overline{\Delta}\tilde{\phi}\right)-\widetilde{V}\cdot\nabla\left(\overline{\Delta}\tilde{\phi}\right)\\ =-\bar{\Omega}_D\partial_y\widetilde{T}+\widetilde{V}_x\partial_x\overline{\Delta}\phi_Z\end{aligned}\tag{20}$$

The direct Fourier transforming of Eq.(20) gives the quasi-linear relation of $\tilde{\phi}$ linking to $\widetilde{T}$:

$$(-i\omega + ik_y\Omega_Z)\,\tilde{\phi}_k = -\frac{\bar{\Omega}_D}{A+\bar{k}_\perp^2} ik_y \widetilde{T}_{\mathbf{k}} - \frac{\partial_x \overline{\Delta}\phi_Z}{A+\bar{k}_\perp^2} ik_y \tilde{\phi}_{\mathbf{k}} \tag{21}$$

where $\bar{k}_\perp^2 = \delta_b^2 k_x^2 + \rho_i^2 k_y^2$ and we dropped the convective nonlinear terms.

Similarly for $\widetilde{T}$, below:

$$\sqrt{2\varepsilon_0}\left(\partial_t + \widetilde{\mathbf{V}}\cdot\nabla + \mathbf{\Omega}_Z\cdot\nabla\right)\widetilde{T} = -i(\omega - \omega_Z - \omega_{*n}^i - \omega_{*T}^i) C_i \tilde{\phi} \tag{22}$$

A trick we used here is to replace $-i(\omega-\omega_Z)\tilde{\phi}$ in the R.H.S. of above with Eq.(21), since $\Omega_Z = \partial_x\phi_Z, \omega_Z = k_y\Omega_Z$. Then the quasi-linear form of the $\widetilde{T}_{\mathbf{k}}$ equation is:

$$\begin{aligned}\left[-i\omega + ik_y\left(\Omega_Z + \frac{C_i}{\sqrt{2\varepsilon_0}}\frac{\bar{\Omega}_D}{A+\bar{k}_\perp^2}\right)\right]\widetilde{T}_{\mathbf{k}} \\ = -\frac{ik_y\tilde{\phi}_{\mathbf{k}}}{\sqrt{2\varepsilon_0}}\left(C_i\frac{\delta_b^2\partial_x^3\phi_Z}{A+\bar{k}_\perp^2} - \partial_x\ln\langle T\rangle\right)\end{aligned} \tag{23}$$

where we dropped the nonlinear convective terms, too. We now have obtained the quasi-linear expressions for both $\tilde{\phi}_{\mathrm{k}}$ and $\widetilde{T}_{\mathrm{k}}$.

In the following context, we will give the formulations of the heat flux and the vorticity flux. The heat flux can be easily obtained from the quasi-linear expressions Eq.(23). But it could be risky to directly use Eq.(21) to obtain quantities like $\langle\tilde{\phi}^2\rangle$, since it will eliminate the important contribution from the zonal vorticity. So we will use the potential vorticity flux to assist to ensure the accuracy, since the full PV $\langle q\rangle + \delta q$ in Eq.(13)-(14) is conserved.

A. Heat flux $\langle\widetilde{V}_x\widetilde{T}\rangle$

The QL heat flux is easy to obtain. First, we have the formula below, from Eq.(23):

$$\begin{aligned}\widetilde{T}_{\mathbf{k}} = \frac{i\widetilde{V}_x(k)}{\omega - k_y\left(\Omega_Z + \frac{C_i}{\sqrt{2\varepsilon_0}}\frac{\bar{\Omega}_D}{A+\bar{k}_\perp^2}\right)}\frac{1}{\sqrt{2\varepsilon_0}} \\ \times\left(C_i\frac{\delta_b^2\partial_x^3\phi_Z}{A+\bar{k}_\perp^2} - \partial_x\ln\langle T\rangle\right)\end{aligned} \tag{24}$$

Then multiply $\widetilde{V}_x(-k)$ on both sides,

$$\begin{aligned}\langle\widetilde{V}_x\widetilde{T}\rangle_k \simeq \frac{i}{\omega - k_y\left(\Omega_Z + \frac{C_i}{\sqrt{2\varepsilon_0}}\frac{\bar{\Omega}_D}{A+\bar{k}_\perp^2}\right)} \\ \times\langle\widetilde{V}_x^2\rangle_k\frac{1}{\sqrt{2\varepsilon_0}}\left(C_i\frac{\delta_b^2\partial_x^3\phi_Z}{A+\bar{k}_\perp^2} - \partial_x\ln\langle T\rangle\right)\end{aligned} \tag{25}$$

The results can be separated into three parts: a response function $R = i/(\omega - k_y\Omega_Z - k_y\bar{\Omega}_D b_k)$, the turbulence intensity $\langle\widetilde{V}_x^2\rangle$, and the drive from both mean temperature gradient and mean vorticity gradient. The form of the response function shows the possibility of a resonant response, which occurs when the dominator vanishes. This will lead to resonant transport which appears in the next section. The turbulence intensity term needs more analysis to be determined. We will use several models and a turbulence intensity evolution equation to address this in the next section. In the third part, since $C_i \sim |q_i\tilde{\phi}/T| \ll 1$, the contributions from the vorticity gradient are seemingly small and are often neglected. But, we keep it here. The important role it plays in $E\times B$ staircase formation will be revealed in the following parts of this paper.

B. Vorticity flux $C_i\langle\widetilde{V}_x\overline{\Delta}\tilde{\phi}\rangle$

The next flux which needs to be calculated is the vorticity flux. Though we already have the $\tilde{\phi}$ evolution equation, directly using $\tilde{\phi}$ or $A\tilde{\phi} - \overline{\Delta}\tilde{\phi}$ to obtain $\widetilde{V}_x\overline{\Delta}\tilde{\phi}$ can lose some important physics. Here we use the potential vorticity flux so as to retain the necessary physics processes. This follows since the total PV in Eq.(13)-(14) is conserved. We have $\langle\widetilde{V}_x\delta q\rangle = \langle\widetilde{V}_x(\widetilde{T} - C_i\overline{\Delta}\tilde{\phi})\rangle = \langle\widetilde{V}_x\widetilde{T}\rangle - C_i\langle\widetilde{V}_x\overline{\Delta}\tilde{\phi}\rangle$, where we set $\tau = 1$. So it's natural to obtain $C_i\langle\widetilde{V}_x\overline{\Delta}\tilde{\phi}\rangle$ from $\langle\widetilde{V}_x\widetilde{T}\rangle - \langle\widetilde{V}_x\delta q\rangle$.

The expression of fluctuating potential vorticity δq can be easily obtained from Eq.(14). Notice we absorbed factors 3/2 and C_i into $\bar{\Omega}_D$ here.

$$\delta q_k = \frac{C_i\bar{\Omega}_D k_y}{\omega - k_y\Omega_Z}\widetilde{T}_k - \frac{i\partial_x\langle q\rangle}{\omega - k_y\Omega_Z}\widetilde{V}_x(k) \tag{26}$$

Then multiply by $\widetilde{V}_x(-k)$ on both sides of above,

$$\begin{aligned}\langle\widetilde{V}_x\delta q\rangle_k \simeq \frac{k_y}{\omega - k_y\Omega_Z}C_i\bar{\Omega}_D\langle\widetilde{V}_x\widetilde{T}\rangle_k \\ - \frac{i}{\omega - k_y\Omega_Z}\langle\widetilde{V}_x^2\rangle_k\left(\frac{1}{\sqrt{2\varepsilon_0}}\partial_x\ln\langle T\rangle - C_i\partial_x\overline{\Delta}\phi_Z\right)\end{aligned}$$

where the definition of mean PV in Eq.(15) is used. The vorticity flux, according to the previous discussion, is ob-

tained below:

$$
\begin{aligned}
&C_i\langle\widetilde{V}_x\overline{\Delta}\tilde{\phi}\rangle = \langle\widetilde{V}_x\widetilde{T}\rangle_k - \langle\widetilde{V}_x\delta q\rangle_k \\
&= \langle\widetilde{V}_x^2\rangle_k \frac{\partial_x \ln\langle T\rangle}{\sqrt{2\varepsilon_0}}\left(1-\frac{1}{\sqrt{2\varepsilon_0}}\frac{1}{A+\bar{k}_\perp^2}\right) \\
&\qquad\times \frac{ik_yC_i\bar{\Omega}_D}{(\omega-k_y\Omega_Z)\left[\omega-k_y\left(\Omega_Z+\frac{C_i}{\sqrt{2\varepsilon_0}}\frac{\bar{\Omega}_D}{A+\bar{k}_\perp^2}\right)\right]} \\
&\quad - C_i\langle\widetilde{V}_x^2\rangle_k\partial_x\overline{\Delta}\phi_Z\left(1-\frac{1}{\sqrt{2\varepsilon_0}}\frac{1}{A+\bar{k}_\perp^2}\right) \\
&\qquad\times \frac{i}{\omega-k_y\left(\Omega_Z+\frac{C_i}{\sqrt{2\varepsilon_0}}\frac{\bar{\Omega}_D}{A+\bar{k}_\perp^2}\right)}
\end{aligned}
$$

For simplicity, we let,

$$
a_k \equiv 1-\frac{1}{\sqrt{2\varepsilon_0}}\frac{1}{A+\bar{k}_\perp^2} = 1-\frac{1}{\sqrt{2\varepsilon_0}}\frac{1}{\frac{\tau}{\sqrt{2\varepsilon_0}}+\bar{k}_\perp^2} > 0
$$

$$
b_k \equiv \frac{C_i}{\sqrt{2\varepsilon_0}}\frac{1}{A+\bar{k}_\perp^2}
$$

Then,

$$
\begin{aligned}
&\langle\widetilde{V}_x\overline{\Delta}\tilde{\phi}\rangle_k \\
&= \frac{\partial_x\ln\langle T\rangle}{\sqrt{2\varepsilon_0}}\frac{ik_yC_i\bar{\Omega}_Da_k\langle\widetilde{V}_x^2\rangle_k}{(\omega-k_y\Omega_Z)(\omega-k_y\Omega_Z-k_yb_k\bar{\Omega}_D)} \\
&\quad - C_i\partial_x\overline{\Delta}\phi_Z\frac{ia_k\langle\widetilde{V}_x^2\rangle_k}{\omega-k_y\Omega_Z-k_yb_k\bar{\Omega}_D}
\end{aligned}
\tag{27}
$$

Equation (27) gives the vorticity flux. It contains the response function, turbulence intensity spectrum, temperature gradient and mean vorticity gradient. Notice the response function for the temperature gradient is different from the response functions for the vorticity gradient. It has two propagator contributions $(\omega-k_y\Omega_Z)$ and $(\omega-k_y\Omega_Z-k_yb_k\bar{\Omega}_D)$.

- From Eq.(21), the response function for $\tilde{\phi}$-like quantities to $\widetilde{T}$ is $i/(\omega-k_y\Omega_Z)$.
- From Eq.(23), the response function for $\widetilde{T}$ to $\tilde{\phi}$-like quantities is $i/(\omega-k_y\Omega_Z-k_yb_k\bar{\Omega}_D)$.

In the correlation $\langle\widetilde{V}_x\overline{\Delta}\tilde{\phi}\rangle$, there is a portion from the $\tilde{\phi}$ linearly responds to $\widetilde{T}$ with the propagator $i/(\omega-k_y\Omega_Z)$. Then the $\widetilde{T}$ linearly responds to a $\tilde{\phi}$-like quantity with the propagator $i/(\omega-k_y\Omega_Z-k_yb_k\bar{\Omega}_D)$. Finally, the linear transfer with two propagators leads to the two contributions of the response function in the first term of the R.H.S of Eq.(27).

The quasi-linear expressions of fluxes Eq.(25) and Eq.(27) are in k space, so we can sum them over k to obtain the real space flux. Before summation, we notice that the response function for the fluxes, for instance, $R = i/(\omega-k_y\Omega_Z-k_y\bar{\Omega}_Db_k)$, can result in resonant transport (when resonance conditions satisfied). This will bring some interesting phenomena, as we will discuss later. Here we take the vorticity flux Eq.(27) as an example to show what the fluxes in real space will be like.

C. Non-res and resonant transport

For the vorticity flux expression Eq.(27), after summation in k space, we can define two transport coefficients as:

$$
\chi_1 = \Re\sum_k\left[\widetilde{V}_x(k)\right]^2\frac{ik_yC_i\bar{\Omega}_Da_k}{(\omega-k_y\Omega_Z)(\omega-k_y\Omega_Z-k_yb_k\bar{\Omega}_D)}
$$

$$
\chi_2 = \Re\sum_k\left[\widetilde{V}_x(k)\right]^2\frac{ia_k}{\omega-k_y\Omega_Z-k_yb_k\bar{\Omega}_D}
$$

where $\Re$ represents the real part. χ_1 corresponds to the contribution from the temperature profile gradient. χ_2 corresponds to the contribution from the mean vorticity gradient. By separating $\omega=\omega_R+i\gamma$, we can isolate the resonant and non-resonant portions of the transport coefficients:

$$
\begin{aligned}
\chi_1^{\mathrm{n-res}} &= \sum_k\left[\widetilde{V}_x(k)\right]^2a_k\frac{|\gamma|k_yC_i\bar{\Omega}_D(2\omega_R-2k_y\Omega_Z-k_yb_k\bar{\Omega}_D)}{|\omega-k_y\Omega_Z|^2|\omega-k_y\Omega_Z-k_yb_k\bar{\Omega}_D|^2} \\
\chi_1^{\mathrm{res}} &= \sum_k\left[\widetilde{V}_x(k)\right]^2a_k\frac{k_yC_i\bar{\Omega}_D\pi\delta(\omega-k_y\Omega_Z-k_yb_k\bar{\Omega}_D)}{\omega-k_y\Omega_Z} \\
&\quad+\sum_k\left[\widetilde{V}_x(k)\right]^2a_k\frac{k_yC_i\bar{\Omega}_D\pi\delta(\omega-k_y\Omega_Z)}{\omega-k_y\Omega_Z-k_yb_k\bar{\Omega}_D}\sim 0 \\
\chi_2^{\mathrm{n-res}} &= \sum_k\left[\widetilde{V}_x(k)\right]^2a_k\frac{|\gamma|}{|\omega-k_y\Omega_Z-k_yb_k\bar{\Omega}_D|^2} \\
\chi_2^{\mathrm{res}} &= \sum_k\left[\widetilde{V}_x(k)\right]^2a_k\pi\delta(\omega-k_y\Omega_Z-k_yb_k\bar{\Omega}_D)
\end{aligned}
$$

Interestingly, after decomposition, we see that the resonant portion of χ_1 has two parts with opposite sign. The exact value of χ_1^{res} depends on the spectrum structure and resonant wave numbers. A cancellation in χ_1^{res} will surely make it smaller than other resonant transport coefficients, i.e. the resonant contribution from temperature gradient is small. So we assume $\chi_1^{\mathrm{res}}\sim 0$ hereafter for simplicity, which means: *in the flux of vorticity, there is no resonant contribution from the temperature gradient.* Therefore, the quasilinear form of vorticity flux may written as:

$$
\langle\widetilde{V}_x\overline{\Delta}\tilde{\phi}\rangle_y = \chi_1^{\mathrm{n-res}}\frac{\partial_x\ln\langle T\rangle}{\sqrt{2\varepsilon_0}} - \left(\chi_2^{\mathrm{n-res}}+\chi_2^{\mathrm{res}}\right)C_i\partial_x\overline{\Delta}\phi_Z \tag{28}
$$

The heat flux can also be obtained directly – there will be both resonant and non-resonant contributions from

temperature gradient and mean vorticity gradient:

$$\begin{aligned}\langle \widetilde{V}_x \widetilde{T}\rangle_y = &-(\chi_3^{\text{n-res}} + \chi_3^{\text{res}})\frac{1}{\sqrt{2\varepsilon_0}}\partial_x \ln\langle T\rangle \\ &+ (\chi_4^{\text{n-res}} + \chi_4^{\text{res}})\frac{C_i}{\sqrt{2\varepsilon_0}}\partial_x \overline{\Delta}\phi_Z\end{aligned} \tag{29}$$

D. Turbulence Intensity evolution equation

In expressions Eq.(25) and Eq.(27), apart from the contribution of profile gradient, there are also contributions from turbulence intensity $\left|\widetilde{V}_x(k)\right|^2$ or equivalently $\langle\tilde{\phi}^2\rangle_k$. In our previous study [41], we already discussed the turbulence intensity evolution characterized by $\langle\tilde{\phi}^2\rangle$, in which we first derived the evolution of $\langle\tilde{U}^2\rangle$, then applied the Green's function and transformed $\langle\tilde{U}^2\rangle \to \langle\tilde{\phi}^2\rangle$. We dropped the effects of $\overline{\Delta}\phi_Z$ and approximated the influence of heat flux with a constant linear growth in Ref.[41]. Now, with the quasi-linear fluxes, we can obtain a more complete turbulence intensity evolution equation characterized by $\langle\tilde{U}^2\rangle$ as below:

$$\begin{aligned}&\frac{1}{2}\left\langle\left(\frac{\partial}{\partial t} + V_Z\cdot\nabla\right)\left(A\tilde{\phi} - \overline{\Delta}\tilde{\phi}\right)^2\right\rangle \\ &= -\bar{\Omega}_D\left\langle\widetilde{T}\left(A\widetilde{V}_x - \delta_b^2\partial_x^2\widetilde{V}_x\right)\right\rangle - \delta_b^2\partial_x\langle\widetilde{V}_x\widetilde{V}_y\rangle\partial_x\overline{\Delta}\phi_Z \\ &+ \frac{1}{2}\left[A\left\langle\nabla\tilde{\phi}^2\times\left(\nabla\overline{\Delta}\tilde{\phi}\right)\cdot\hat{z}\right\rangle + \left\langle\nabla\left(\overline{\Delta}\tilde{\phi}\right)^2\times\nabla\tilde{\phi}\cdot\hat{z}\right\rangle\right]\end{aligned} \tag{30}$$

Equation above comes from Eq.(20), which is fundamentally the evolution equation for potential enstrophy $\langle\tilde{U}^2\rangle$ (derived from potential vorticity $\tilde{U} \equiv A\tilde{\phi} - \overline{\Delta}\tilde{\phi}$). The first term in the R.H.S. of Eq.(30) is similar to the heat flux, the second term is related to vorticity flux (or Reynolds stress by the Taylor Identity) and mean vorticity gradient. The third term is a complex nonlinear term. Since we already obtained the heat flux and vorticity flux in a previous subsection, the first two terms in the R.H.S. of Eq.(30) can be dealt using the same approach. More details can be found in Appendix B. As for the third term, from our previous study [41], it contains nonlinear diffusion and nonlinear scattering effects. We apply the model of Ref.[41] here and simplify it to a nonlinear diffusion term $\partial_x D_U \partial_x\langle\tilde{U}^2\rangle$ and a nonlinear damping term $\langle\tilde{U}^2\rangle\nu_{\text{NL}}/l_x^2$, where $D_U \propto \langle\tilde{\phi}^2\rangle$, ν_{NL} is a parameter for nonlinear damping, l_x is limited by gyro-radius and banana orbit width. The damping represents transfer to small scale dissipation. We will try to improve this approximation of the third term in future work. Applying all these approximations to Eq.(30), we obtain Eq.(31) as:

$$\begin{aligned}&\frac{1}{2}\frac{\partial}{\partial t}\langle\tilde{U}^2\rangle \\ &= \frac{\partial}{\partial x}D_U\frac{\partial}{\partial x}\langle\tilde{U}^2\rangle - \frac{\nu_{\text{NL}}}{l_x^2}\langle\tilde{U}^2\rangle \\ &+ \frac{\bar{\Omega}_D}{\sqrt{2\varepsilon_0}}(\chi_5^{\text{n-res}} + \chi_5^{\text{res}})\frac{\partial}{\partial x}\langle T\rangle \\ &- \frac{\bar{\Omega}_D}{\sqrt{2\varepsilon_0}}C_i(\chi_6^{\text{n-res}} + \chi_6^{\text{res}})\frac{\partial}{\partial x}\left(\overline{\Delta}\phi_Z\right) \\ &- \frac{1}{C_i}\chi_1^{\text{n-res}}\left(\frac{\partial}{\partial x}\frac{\ln\langle T\rangle}{\sqrt{2\varepsilon_0}}\right)\left[\frac{\partial}{\partial x}\left(\overline{\Delta}\phi_Z\right)\right] \\ &+ \left(\chi_2^{\text{n-res}} + \chi_2^{\text{res}}\right)\left[\frac{\partial}{\partial x}\left(\overline{\Delta}\phi_Z\right)\right]^2\end{aligned} \tag{31}$$

where the expressions for χ_5 and χ_6 can be found in the Appendix B. After solving Eq.(31) and obtaining $\langle\tilde{U}^2\rangle$, we use the Green's function to obtain $\langle\tilde{\phi}^2\rangle = \mathcal{G}_2 \otimes \langle\tilde{U}^2\rangle$. This will give us the turbulence intensity we need to calculate the transport coefficients.

Recalling the mean profile evolution equation at the beginning of this section Eq.(17)-(18), we put the vorticity flux and heat flux into them to obtain:

$$\begin{aligned}\frac{\partial}{\partial t}\left(\overline{\Delta}\phi_Z\right) = &-\frac{\partial}{\partial x}\left(\frac{1}{C_i}\chi_1^{\text{n-res}}\frac{\partial}{\partial x}\frac{\ln\langle T\rangle}{\sqrt{2\varepsilon_0}}\right) \\ &+ \frac{\partial}{\partial x}\left[\left(\chi_2^{\text{n-res}} + \chi_2^{\text{res}} + \nu_c\right)\frac{\partial}{\partial x}\overline{\Delta}\phi_Z\right]\end{aligned} \tag{32}$$

$$\begin{aligned}\frac{\partial}{\partial t}\ln\langle T\rangle = &-\frac{\partial}{\partial x}\left[C_i\left(\chi_4^{\text{n-res}} + \chi_4^{\text{res}}\right)\frac{\partial}{\partial x}\left(\overline{\Delta}\phi_Z\right)\right] \\ &+ \frac{\partial}{\partial x}\left[\left(\chi_3^{\text{n-res}} + \chi_3^{\text{res}} + \chi_{\text{neo}}\right)\frac{\partial}{\partial x}\ln\langle T\rangle\right]\end{aligned} \tag{33}$$

Here we added two terms – ν_c is collisional dissipation for mean flow, and χ_{neo} is the neoclassical thermal diffusion. In our model, both terms are small compared to turbulent transport. With Eq.(31)-(33), the turbulence-profile evolution system we need for studying the $E\times B$ staircase begins to take shape. But obviously, there are many transport coefficients to be determined. The system is not yet solvable. The next step is further simplification of the transport coefficients.

IV. MODELLING THE TRANSPORT COEFFICIENTS

We obtained the flux required for mean profile evolution in previous section. As we can see, there are still a lot of transport coefficients that need to be simplified. The goal of this section is to construct an appropriate model of the transport coefficients and determine the resonance condition. Let's continue to focus on χ_3 as an example.

Results for other coefficients can be found in Appendix B.

$$\chi_3^{\mathrm{n-res}} = \sum_k \left[\widetilde{V}_x(k)\right]^2 \frac{|\gamma|}{|\omega - k_y\Omega_Z - k_y b_k \bar{\Omega}_D|^2} \tag{34}$$

$$\chi_3^{\mathrm{res}} = \sum_k \left[\widetilde{V}_x(k)\right]^2 \pi\delta(\omega - k_y\Omega_Z - k_y b_k \bar{\Omega}_D) \tag{35}$$

The straightforward way to simplify the expressions above is by working out the analytical expression for the summation or integral. To implement this approach, we will need two ingredients: the dispersion relation $\omega(k)$ and the spectrum $\langle\tilde{\phi}^2\rangle_k$. Luckily, these two conditions can be supplied by appropriate models.

The dispersion function can be obtained from the Darmet model Eq.(4)-(5), as in Appendix A. By numerically solving this dispersion function, we then obtain the dispersion relation, which can be modeled approximately as below (more details in Eq.(A16), Eq.(A17) in the Appendix A):

$$\omega_R = R\Omega_D k_y, \quad \gamma = \Lambda R\Omega_D k_y(k_{y,\max} - k_y) \tag{36}$$

Here the real frequency is simply proportional to k_y, and the growth rate is modelled as a parabolic function of k_y. R is a constant ~ 2.3, and Λ and $k_{y,\max}$ are parameters fit to the numerical results. For convenience, we set $\Lambda = \rho_i/\sigma$, $k_{y,\max} = 1/(\mu\rho_i)$. Since the effect of k_x and κ_T on the real frequency is small, we dropped their dependence here, for simplicity.

For convenience, after truncating at high wave numbers, we can apply a bi-Lorentz spectrum[53], here:

$$|\tilde{\phi}|^2_{k_x,k_y} = \frac{|\tilde{\phi}_0|^2}{\pi^2\Delta k_x\Delta k_y} \times \frac{1}{\left[1+\left(\frac{k_x-k_{r0}}{\Delta k_x}\right)^2\right]\left[1+\left(\frac{k_y-k_{y0}}{\Delta k_y}\right)^2\right]} \tag{37}$$

To work out the integral, we need to connect the two models above. There are two sets of parameters for the models,

1. $(k_{x,\max}, k_{y,\max}, \Lambda)$ for the dispersion relation
2. $(k_{x0}, k_{y0}, \Delta k_x, \Delta k_y)$ for the spectrum

We can connect the second set of parameters to the first set by setting:

$$k_{x0} = \alpha_x k_{x,\max}, \quad \Delta k_r = \beta_x k_{x,\max} \tag{38}$$

$$k_{y0} = \alpha_y k_{y,\max}, \quad \Delta k_y = \beta_y k_{y,\max} \tag{39}$$

We should have $\alpha_{x,y} \ll 1$, $\beta_{x,y} < 1$. We can take $\alpha = 0$ for simplicity. These connection parameters will not affect our conclusions. And again, we emphasize we set $\Lambda \sim \rho_i/\sigma, k_{y,\max} = 1/(\mu_y\rho_i)$, for convenience. With all the above, the dispersion relation model Eq.(36) and spectrum model Eq.(37) now can be used in calculating the transport coefficients like Eq.(34)-(35). Let's continue our journey to simplify χ_3.

A. Simplification of non-resonant coefficients

For coefficient $\chi_3^{\mathrm{n-res}}$, the summation Eq.(34) in k will be transformed into an integral, then we plug the models Eq.(36) into it. $|\tilde{\phi}|^2_{k_x,k_y}$ is a bi-Lorentz spectrum Eq.(37). The result reads as:

$$\chi_3^{\mathrm{n-res}} = 2\int_0^{k_{y,\max}}\int_0^{k_{x,\max}} |\tilde{\phi}|^2_{k_x,k_y} \times \frac{\Lambda k_y(k_{y,\max}-k_y)}{R\Omega_D\left[1+\Lambda^2\left(k_{y,\max}-k_y\right)^2\right]}\mathrm{d}k_x\mathrm{d}k_y \tag{40}$$

where we set the upper boundary of integral as $k_{x,\max}$ and $k_{y,\max}$. Then using the connection parameters we defined, we can work out the integral analytically. The result is long and tedious, as shown on the Appendix B. But luckily, we find that the principal term in the result is determined by the $\mu^2\sigma^2$ related terms. From the dispersion relation (in Appendix A), we know $\mu\sigma$ is between $\mathcal{O}(1) - \mathcal{O}(10)$. So we keep the largest terms in $\mu^2\sigma^2$, then the ultimate approximation for $\chi_3^{\mathrm{n-res}}$ is:

$$\chi_3^{\mathrm{n-res}} \sim \frac{|\tilde{\phi}_0|^2\mu^2\sigma^2}{\Omega_D\rho_i\left[(\mu^2\sigma^2+1+\beta^2)^2\right]} \tag{41}$$

As for the other transport coefficients, we normalize all of them to $\chi_3^{\mathrm{n-res}}$, then we obtain the list below:

$$\chi_1^{\mathrm{n-res}} = \vartheta\chi_3^{\mathrm{n-res}} \tag{42}$$

$$\chi_2^{\mathrm{n-res}} = \vartheta\chi_3^{\mathrm{n-res}} \tag{43}$$

$$\chi_4^{\mathrm{n-res}} = \sqrt{2\varepsilon_0}(\tau-\vartheta)\chi_3^{\mathrm{n-res}} \tag{44}$$

$$\chi_5^{\mathrm{n-res}} = \frac{1}{\sqrt{2\varepsilon_0}}(\tau+\vartheta)\chi_3^{\mathrm{n-res}} \tag{45}$$

$$\chi_6^{\mathrm{n-res}} = \chi_3^{\mathrm{n-res}} \tag{46}$$

Where $\vartheta \equiv \sqrt{2\varepsilon_0}\Theta_{\max}C < 1$ is a constant we defined in Appendix B. Now, all non-resonant transport coefficients are simplified.

B. Simplification of resonant coefficients

For the resonant transport coefficients like χ_3^{res}, we just need to find the resonant condition, i.e. the solution of the δ function, and replace those resonant k_{res} in the spectrum function. As in the previous subsection, we normalize all other coefficients to χ_3^{res}.

1. *Resonant condition*

The resonance condition in Eq.(35) is:

$$\delta\left(\omega_R - k_y\Omega_Z - \frac{C_i\overline{\Omega}_D k_y}{\tau+\sqrt{2\epsilon_0}\left(\delta_b^2k_x^2+\rho_i^2k_y^2\right)}\right) \tag{47}$$

Here $\overline{\Omega}_D = 3\Omega_D/(2C_i)$, ω_R is the real frequency of modes. We know from the dispersion relation in Appendix A, that the real frequency can be well fit by:

$$\omega_R = \frac{R_1 k_y \Omega_D}{1 + R_2(\rho_i^2 k_y^2 + \delta_b^2 k_x^2)} \simeq R k_y \Omega_D \tag{48}$$

Here R_2 is much smaller than 1, $R \approx 2.36$, as shown in Eq.(A16). Putting the expression for real frequency above, into Eq.(47), we can obtain the $k_{\rm res}$ that match the resonant condition. Notice the match condition is determined primarily by $\delta_b^2 k_x^2 + \rho_i^2 k_y^2$, so we can define it as a quantity like:

$$\Theta_{\rm res} \equiv \delta_b^2 k_{x,\rm res}^2 + \rho_i^2 k_{y,\rm res}^2 \tag{49}$$

Then from the resonance condition Eq.(47), we know the resonant wave numbers (k_x, k_y) must satisfy:

$$\Theta_{\rm res} = \frac{\Omega_D(R\tau - 1.5) - \tau\Omega_Z}{\sqrt{2\varepsilon_0}\,(\Omega_Z - R\Omega_D)} \tag{50}$$

After looking carefully at the resonance condition above, we notice all the parameters on the R.H.S. are constants, except $\Omega_Z = \partial_x \phi_Z$. *Note here Ω_Z connects the resonance condition to the mean flow profile!* We plot the relation between $\Theta_{\rm res}$ and Ω_Z in FIG. 1. Different lines in FIG. 1 represent the varying of fit parameters R, for testing parameter sensitivity.

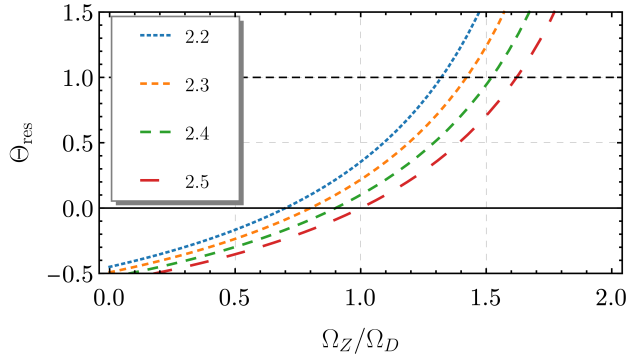

FIG. 1: $\Theta_{\rm res}$ and Ω_Z. On a range of Ω_Z the resonance can exist. The threshold for resonance existence is approximately $\Omega_Z \gtrsim \Omega_D$. And when Ω_Z is too big ($\sim 1.5\Omega_D$), the resonance condition $\Theta_{\rm res} > 1$ is not satisfied. Different lines represent the variation of R in Eq.(36).

From the dispersion relation Eq.(A15), there is

$$\Theta_{\rm max} \equiv \delta_b^2 k_{x,\rm max}^2 + \rho_i^2 k_{y,\rm max}^2 = \frac{1}{\mu_x^2} + \frac{1}{\mu_y^2} \sim 1 \tag{51}$$

Therefore all the other Θ must satisfy $\Theta < \Theta_{\rm max} \sim 1$, including $\Theta_{\rm res}$. As we show in the FIG. 1, to make resonance possible, there must be $0 < \Theta_{\rm res} < 1$, thus Ω_Z/Ω_D must lie approximately between 1 and 1.5. So as long as $1 < \Omega_Z/\Omega_D < 1.5$, there will be some $(k_{x,\rm res}, k_{y,\rm res})$ to satisfy the resonance condition mentioned above. Alternatively, *$1 < \Omega_Z/\Omega_D < 1.5$ can be regarded as the resonance condition!*

The mechanism to connect the resonance condition to the $E \times B$ mean toroidal flow is simple. In this paper, the trapped ion procession velocity Ω_D is set as a constant. The energy dependence is absorbed by normalization $\hat{\Omega}_D = \Omega_D T_0/\omega_0$ in section II. The fluctuating energy dependence in precession velocity is reflected by the terms like $\Omega_D \widetilde{T}$, for example the first term in the R.H.S. of Eq.(7). The phase velocity of the trapped ion mode is $R\Omega_D$, where $R \simeq 2.36$ from Appendix A. Notice there is a natural gap between the precession velocity and phase velocity. When $E \times B$ mean flow $\Omega_Z \sim \Omega_D$, the trapped ion precession will resonant with TIM with the additional increment of the Doppler shift from the mean flow.

2. *Simplification of coefficients*

Returning to those resonant transport coefficients $\chi_3^{\rm res}$, when the condition $1 < \Omega_Z/\Omega_D < 1.5$ is satisfied, there will be some $(k_{x,\rm res}, k_{y,\rm res})$ which fullfil the resonance condition Eq.(50). Rewriting the summation in Eq.(35) as an integral, and putting these $(k_{x,\rm res}, k_{y,\rm res})$ into it, we obtain Eq.(B17) as shown in Appendix B. Let $\vartheta_{\rm res} = \sqrt{2\varepsilon_0}\Theta_{\rm res}$, and we finally have the list for resonant transport coefficients, as below:

$$\chi_2^{\rm res} \sim \vartheta_{\rm res}\chi_3^{\rm res} \tag{52}$$

$$\chi_3^{\rm res} = |\tilde{\phi}_0|^2 k_{y,\rm res}^2 \frac{\beta^2}{\beta^2 + \mu^2\Theta_{\rm res}} \frac{\mu_y \rho_i}{|\beta_y\,(\Omega_Z + \Omega_D)|} \tag{53}$$

$$\chi_4^{\rm res} \sim \sqrt{2\varepsilon_0}(1 - \vartheta_{\rm res})\chi_3^{\rm res} \tag{54}$$

$$\chi_5^{\rm res} \sim \frac{1}{\sqrt{2\varepsilon_0}}(1 + \vartheta_{\rm res})\chi_3^{\rm res} \tag{55}$$

And remember that all the resonant transport coefficients exist only when the condition $1 < \Omega_Z/\Omega_D < 1.5$ is satisfied.

Now, we already have all the turbulent transport coefficients that appear in the model Eq.(31)-(33). Theoretically, we can solve for the profile evolution with all the ingredients including. For the convenience of calculation, we now introduce a unified χ model.

C. A unified χ model

Let's extract the turbulence intensity from the coefficients. Here we still take χ_3 as an example. We define

two quantities $\chi^{\rm n}$ and $\chi^{\rm r}$:

$$\chi_3^{\rm n-res} = \frac{|\tilde{\phi}_0|^2\mu^2\sigma^2}{\Omega_D\rho_i\left[\left(\mu^2\sigma^2+1+\beta^2\right)^2\right]} \equiv \chi^{\rm n}|\tilde{\phi}_0|^2 \tag{56}$$

$$\chi_3^{\rm res} = \frac{|\tilde{\phi}_0|^2 k_{y,\rm res}^2\beta^2}{\beta^2+\mu^2\Theta_{\rm res}}\frac{\mu_y\rho_i}{|\beta_y\left(\Omega_Z+\Omega_D\right)|} \equiv \chi^{\rm r}|\tilde{\phi}_0|^2 \tag{57}$$

$\chi_3^{\rm res}$ exists if and only if $\Omega_D < \Omega_Z < 1.5\Omega_D$. As for other coefficients, we simply set $\vartheta = \vartheta_{\max} = \vartheta_{\rm res}$. Considering $\mu^2\sigma^2 \sim 10$, there should be

$$\chi^{\rm r}/\chi^{\rm n} \sim \frac{\left(\mu^2\sigma^2+1+\beta^2\right)^2}{\mu^2\sigma^2} \sim \mathcal{O}(10)-\mathcal{O}(10^2) \tag{58}$$

In another word, the resonant coefficients are approximately 10 to 100 times bigger than the non-resonant coefficients. From the definition, we know that $\mu\sigma = (\Lambda k_{y,\max})^{-1}$, so the ratio of resonant to non-resonant transport is roughly the square of the ratio between real frequency and growth rate:

$$\chi^{\rm r}/\chi^{\rm n} \sim \frac{1}{\Lambda^2 k_{y,\max}^2} \sim \frac{\Omega_D^2}{\Lambda^2\Omega_D^2 k_{y,\max}^2} \sim \frac{\omega_R^2}{\gamma^2} \tag{59}$$

Conventional wisdom would give $\chi^{\rm r}/\chi^{\rm n} \sim \omega_R/\gamma$ here. The difference comes from the calculation of Lorentzian spectrum with TIM dispersion relation, as we did, in which the mode structure plays a larger role than for the usual quasi-linear results. With this additional information concerning the ratio, it would be convenient to define a piecewise function $\chi \equiv (\chi^{\rm n}+\chi^{\rm r})|\tilde{\phi}_0|^2$ with *tanh* functions as FIG.2, where $\chi^{\rm n}=1$, $\chi^{\rm r}=100$. This unifies the non-resonant and resonant transport coefficients Eq.(56) and Eq.(57). For the consideration of smooth numerical calculation, we set a "bandwidth" $w_\Omega = 0.2$ around the thresholds $\Omega_Z = \Omega_D$, as in FIG.2.

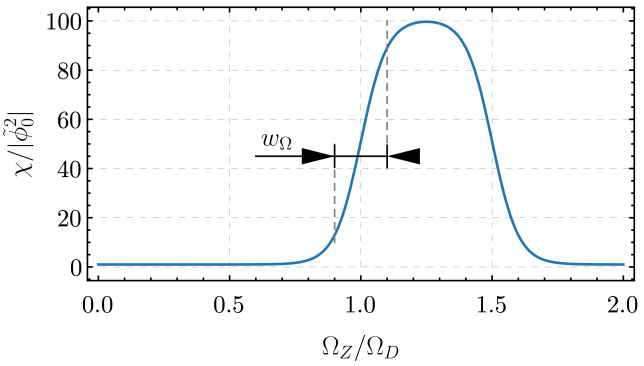

FIG. 2: A piecewise continuous function of χ v.s. Ω_Z as a transport coefficient model. When Ω_Z is not in the range of resonant condition, $\chi = \chi^{\rm n}|\tilde{\phi}_0|^2$; when $1 < \Omega_Z/\Omega_D < 1.5$, $\chi = \chi^{\rm r}|\tilde{\phi}_0|^2$. w_Ω is the "bandwidth" of the threshold we set for convenience.

D. On the Near Marginality Hypothesis

In this subsection, we give a short discussion on the problem of "near marginality". The resonant transport coefficients we defined in this paper are large enough to quickly relax κ_T (or $1/L_T$) to a very low level, and even below the critical gradient $\kappa_T^{\rm c}$ for TIM instability (as determined in Appendix A). This brings a causality problem: when the temperature gradient is not big enough to excite the instability and turbulence, there should be no turbulent transport coefficients. There are two possible ways to address this issue.

The first way is to ansatz that the physical processes will organize a so-called *near-marginal* state of the profile. When $\kappa_T < \kappa_T^{\rm c}$, all the turbulent transport coefficients $\to 0$ and the neoclassical transport is not negligible. On the contrary, when $\kappa_T \gtrsim \kappa_T^{\rm c}$, turbulent transport coefficients increase dramatically. This is equivalent to the oft-encountered "stiff profile state". Then the temperature profile gradient will balance dynamically near the critical value $\kappa_T^{\rm c}$. Of course, further detailed study is required to determine "how near is 'near'?"

The second way is to consider the nonlocality of turbulence. Noticing the arguments above are all based upon the picture of local turbulence – the local gradient excites local instability; local instability then evolves to local turbulence, which feeds back upon the local gradient. But there is evidence for nonlocality in plasma turbulence[41, 54–57]. From this perspective, $\kappa_T < \kappa_T^{\rm c}$ locally will not necessarily cause a zero level of turbulence and turbulent transport coefficients, because nonlocal excitation or turbulence spreading can bring a finite level of turbulence to regions with $1/L_T \to 0$.

A quantitative understanding of near marginality of profiles is an unsolved question, that requires extensive simulation and experimental studies, which are beyond the scope of this paper. So we introduce the hypothesis in this paper that: *the regions of low ∇T caused by resonant transport in our model are actually at a near marginal state, for which the temperature gradient is near the threshold of instability Eq.*(A14).

V. PROFILE EVOLUTION: FORMATION OF $E\times B$ STAIRCASES

So far, we have obtained the fluxes and transport coefficient models required for solving the evolution equations (31)-(33). The whole process is summarized in the derivation flow charts FIG. 3 and FIG. 4. The next steps are solving the system and studying the evolution of the profiles. More specifically, we will introduce a constant flux drive at the boundaries. This yields a so-called flux-driven system. Under certain conditions, the system will evolve a quasi-periodic pattern of profiles. The basic feedback loops in this system are discussed. Then we determine when the staircase forms and the parameters that control the basic characteristics of staircase.

$$\frac{\partial}{\partial t}\ln\langle T\rangle = -\sqrt{2\varepsilon_0}\partial_x\underline{\langle\widetilde{V}_x\widetilde{T}\rangle_y} + \chi_{\rm neo}\partial_x^2\ln\langle T\rangle$$
$$\downarrow$$
$$\langle\widetilde{V}_x\widetilde{T}\rangle_k$$
$$\downarrow$$
$$\sim R\left(\omega - k_y\Omega_Z - b_k\bar{\Omega}_D\right)\langle\widetilde{V}_x^2\rangle_k\left[\partial_x\overline{\Delta}\phi_Z(\dots) - \partial_x\ln\langle T\rangle(\dots)\right]$$
$$\downarrow$$
$$(\chi_4^{\rm n-res} + \chi_4^{\rm res})\partial_x\overline{\Delta}\phi_Z - (\chi_3^{\rm n-res} + \chi_3^{\rm res})\partial_x\ln\langle T\rangle$$
$$\chi \text{ model}\downarrow$$
Equation (61)

FIG. 3: Derivation flow chart for heat flux. From the evolution equations of fluctuation quantities Eq.(7) and Eq.(9), we construct the quasi-linear expression for the heat flux. Both the mean vorticity gradient and the temperature gradient contribute to the heat flux. Res- and non-resonant portion of the transport coefficients are separated. A transport coefficient model is used to unify all coefficients and simplify the expressions. Quasi-linear heat flux close the evolution equation of $\ln\langle T\rangle$ and results in Eq.(61).

$$\frac{\partial}{\partial t}\left[\overline{\Delta}\phi_Z\right] = -\partial_x\underline{\left\langle\widetilde{V}_x\overline{\Delta}\tilde{\phi}\right\rangle_y} + \nu_c\partial_x^2\overline{\Delta}\phi_Z$$
$$\downarrow$$
$$\langle\widetilde{V}_x\overline{\Delta}\tilde{\phi}\rangle_k = -\underline{\langle\widetilde{V}_x\delta q\rangle_k} + \langle\widetilde{V}_x\widetilde{T}\rangle_k$$
$$\downarrow$$
$$R\left(\omega - k_y\Omega_Z\right)\langle\widetilde{V}_x\widetilde{T}\rangle_k(\cdots)$$
$$-R\left(\omega - k_y\Omega_Z\right)\langle\widetilde{V}_x^2\rangle_k\times$$
$$\left[\partial_x\ln\langle T\rangle(\dots) - \partial_x\overline{\Delta}\phi_Z(\dots)\right]$$
$$\downarrow$$
$$R\left(\omega - k_y\Omega_Z\right)R\left(\omega - k_y\Omega_Z - k_yb_k\bar{\Omega}_D\right)\langle\widetilde{V}_x^2\rangle_k\partial_x\ln\langle T\rangle(\dots)$$
$$-R\left(\omega - k_y\Omega_Z - k_yb_k\bar{\Omega}_D\right)\langle\widetilde{V}_x^2\rangle_k\partial_x\overline{\Delta}\phi_Z(\dots)$$
$$\downarrow$$
$$\chi_1^{\rm n-res}\frac{\partial_x\ln\langle T\rangle}{\sqrt{2\varepsilon_0}} - \left(\chi_2^{\rm n-res} + \chi_2^{\rm res}\right)\partial_x\overline{\Delta}\phi_Z$$
$$\chi \text{ model}\downarrow$$
Equation (60)

FIG. 4: Derivation flow chart for vorticity flux. Quasi-linear expression for vorticity flux is constructed from the fluctuation evolution equations Eq.(7) and Eq.(9). Potential vorticity flux is used to assist the derivation. Res- and non-resonant portions of the transport coefficients are separated. A transport coefficient model is used to unify all coefficients and simplify expressions. Quasi-linear vorticity flux close the evolution equation of $\overline{\Delta}\phi_Z$ and results in Eq.(60).

A. Equations and boundary conditions

As the derivation flow charts show, we put all the simplifications of coefficients Eq.(56), Eq.(57) and fluxes into the profile evolution equations. Finally, we obtain:

$$\frac{\partial}{\partial t}\left(\overline{\Delta}\phi_Z\right) = -\frac{\partial}{\partial x}\left(\frac{1}{C_i}\vartheta\chi^{\rm n}\frac{\partial}{\partial x}\frac{\ln\langle T\rangle}{\sqrt{2\varepsilon_0}}\right) + \frac{\partial}{\partial x}\left[\vartheta\chi\delta_b^2\frac{\partial^3}{\partial x^3}\phi_Z\right] + \nu_c\frac{\partial^2}{\partial x^2}\overline{\Delta}\phi_Z \quad (60)$$

$$\frac{\partial}{\partial t}\ln\langle T\rangle = -\frac{\partial}{\partial x}\left[C_i\sqrt{2\varepsilon_0}(1-\vartheta)\chi\frac{\partial}{\partial x}\left(\overline{\Delta}\phi_Z\right)\right] + \frac{\partial}{\partial x}\left[\chi\frac{\partial}{\partial x}\ln\langle T\rangle\right] + \chi_{\rm neo}\frac{\partial^2}{\partial x^2}\ln\langle T\rangle \quad (61)$$

Here $\chi(\Omega_Z)$ is the piecewise function we defined that includes resonant and non-resonant transport, as FIG.2. Boundary conditions are necessary for solving the equations above. Here we choose the simplest ones:

$$\frac{\partial}{\partial x}\overline{\Delta}\phi_Z\Big|_{\rm B} = 0 \quad (62)$$

$$\frac{\partial}{\partial x}\ln\langle T\rangle\Big|_{\rm B} \equiv \kappa_T^{\rm B} = \text{Const.} \quad (63)$$

$$\frac{\partial}{\partial x}\langle\tilde{U}^2\rangle\Big|_{\rm B} = 0, \quad \text{or} \quad \frac{\partial}{\partial x}\langle\tilde{\phi}^2\rangle\Big|_{\rm B} = 0 \quad (64)$$

Most gradients of quantities at boundaries ($x = 0$ and $x = 1$) are set to 0. Notice the temperature gradient at the boundaries is set to a control parameter, i.e. $\kappa_T^{\rm B}$, where $\kappa_T \equiv \partial_x\ln\langle T\rangle$. So the boundary heat flux will drive the system evolution, corresponding to a "Flux-driven" system. The boundary temperature gradient $\kappa_T^{\rm B} \equiv \kappa_T^{\rm I} + \Delta\kappa_T$ contains the initial value $\kappa_T^{\rm I}$ and the increment $\Delta\kappa_T$. Since $\Delta\kappa_T$ determines the increment of heat flux driven at the boundaries, it can be called the "net drive" or "free energy" that passes through the system.

Recall that we used the piecewise function $\chi \equiv (\chi^{\rm n} + \chi^{\rm r})|\tilde{\phi}_0|^2$ as the coefficient model, as in FIG. 2. Here, in order to keep the notation concise, we hereafter take the $\chi^{\rm n}$ that appears in the following equations to be $\chi^{\rm n}|\tilde{\phi}_0|^2$. χ is a function of $\Omega_Z = \partial_x\phi_Z$, therefore we need to set boundary conditions for Ω_Z, which are:

$$\Omega_Z\Big|_{\rm B} = 0 \quad (65)$$

Note that χ is a function of the turbulence intensity $|\tilde{\phi}_0|^2$. To obtain $|\tilde{\phi}_0|^2$, we include the evolution equation for

$\langle\tilde{U}^2\rangle$ from Eq.(31):

$$\begin{aligned}\frac{1}{2}\frac{\partial}{\partial t}\langle\tilde{U}^2\rangle = &\frac{\partial}{\partial x}D_U\frac{\partial}{\partial x}\langle\tilde{U}^2\rangle - \frac{3}{2}\frac{\Omega_D}{\sqrt{2\varepsilon_0}}\chi\frac{\partial}{\partial x}\left(\overline{\Delta}\phi_Z\right)\\ &+\frac{3}{2}\frac{\Omega_D}{2\varepsilon_0 C_i}(1+\vartheta)\chi\frac{\partial}{\partial x}\ln\langle T\rangle\\ &-\frac{1}{C_i}\vartheta\chi^{\mathrm{n}}\left(\frac{\partial}{\partial x}\frac{\ln\langle T\rangle}{\sqrt{2\varepsilon_0}}\right)\left[\frac{\partial}{\partial x}\left(\overline{\Delta}\phi_Z\right)\right]\\ &+\vartheta\chi\left[\frac{\partial}{\partial x}\left(\overline{\Delta}\phi_Z\right)\right]^2 - \frac{\nu_{\mathrm{NL}}}{l_x^2}\langle\tilde{U}^2\rangle^2\end{aligned} \tag{66}$$

Here ν_{NL} is a parameter for nonlinear saturation of turbulence, and l_x is the radial scale length of turbulence intensity[41]. Then we obtain $\langle\tilde{\phi}^2\rangle$ from $\langle\tilde{U}^2\rangle$ by:

$$\langle\tilde{\phi}^2\rangle = \int_{-\infty}^{\infty} G_2(x-x')\langle\tilde{U}^2\rangle(x')\,\mathrm{d}x' \tag{67}$$

here the Green's function is defined as:

$$\begin{aligned}G_2(x) &= \mathscr{F}^{-1}\left\{\frac{1}{\left(A+k^2\right)^2}\right\}\\ &= \frac{1}{2}\sqrt{\frac{\pi}{2A^3}}\left(e^{-\sqrt{A}|x|}+\sqrt{A}|x|e^{-\sqrt{A}|x|}\right)\end{aligned} \tag{68}$$

with $A \equiv \tau/\sqrt{2\varepsilon_0}$. Boundary conditions for turbulence intensity are set in Eq.(64). Then we assume $|\tilde{\phi}_0|^2 \sim \langle\tilde{\phi}^2\rangle$ here.

We expect the saturated turbulence intensity to be roughly around the gyro-Bohm level, i.e. $\langle\tilde{\phi}^2\rangle \sim \delta_b^2$ and $\langle\tilde{U}^2\rangle \sim \delta_b^2$. From the usual turbulence spreading picture, turbulence extract energy from the gradient and saturated by nonlinear damping. Such a picture corresponds to the balance between the third and sixth terms in the R.H.S. of Eq.(66). To satisfy the expectation of gyro-Bohm-level turbulence, we can use this balance relation and set the parameters in the calculation as:

$$l_x \sim \delta_b \tag{69}$$

$$\nu_{\mathrm{NL}} \sim \frac{3}{2}\frac{\Omega_D}{2\varepsilon_0 C_i}(1+\vartheta) \tag{70}$$

Finally, the evolution equations for profiles Eq.(60), Eq.(61) and the turbulence intensity evolution Eq.(66), the boundary conditions Eq.(62)-(65) and transport coefficient model in FIG. 2 constitute the complete system we study. The definitions for main quantities in Eq.(60)-Eq.(66) are listed in Table I. We will use numerical methods to solve it.

B. Numerical results and basic behaviors of profiles

We choose the "method of lines" to discretize the equations, then solve the set of differential-algebraic equations we obtained using the parameters listed in Table II. Here setting $\nu_{\mathrm{NL}} = 40$ leads to a saturated $\langle\tilde{\phi}^2\rangle \sim \delta_b^2$ as we mentioned in Eq.(70). Then we have $\chi \simeq (\chi^{\mathrm{n}}+\chi^{\mathrm{r}})\delta_b^2$. Both ν_c and χ_{neo} are set to be smaller than the non-resonant turbulent diffusivity with fixed ratios, as shown in Table II. The initial condition for $\ln\langle T\rangle$ is set with a constant gradient equal to 1. The initial conditions for $\langle\tilde{U}^2\rangle$ and $\langle\tilde{\phi}^2\rangle$ are set at a small quantity $\delta_b^2/10$. Initial values for other quantities are set to 0. The results are given in FIG. 5. The temperature profile evolves into a pattern of quasi-periodic corrugations in radius, which is accompanied by patterning in the $E\times B$ mean flow profile, i.e. *the system evolves to an $E\times B$ staircase.* Since the formation of the pattern is fast, we plot the evolution of $E\times B$ mean flow and temperature gradient with an extended time scale in FIG. 6 to show more details. Noticing in FIG. 5 (e)-(f), while turbulence intensity characterized by $\langle\tilde{U}^2\rangle$ has corrugations and patterns, the turbulence intensity characterized by $\langle\tilde{\phi}^2\rangle$ manifests only slight corrugations. This is because after convolution with the Green's function Eq.(68), the corrugations in $\langle\tilde{\phi}^2\rangle$ are smoothed. And remember $\langle\tilde{\phi}^2\rangle$ is the actual quantity that used in calculating transport coefficients. *So the variation of turbulence intensity is not the primary cause of staircase formation here.*

A set of time slices of the profiles are shown in FIG. 7. We can notice there are two distinct states in the temperature profile in FIG. 7(c). One is nearly flat, other is steeper. The two states are alternatively arranged, sequentially in space, and together form a staircase-like pattern! We named those regions with flat temperature profile type II regions, and the regions with steeper profile type I regions, as we show in FIG. 7. In type II regions, the mean vorticity profile is also flatter, and more importantly, Ω_Z/Ω_D is near the threshold for resonant transport, as shown in FIG. 7(a). *Therefore, in Region II, resonant transport is dominant. Meanwhile, in Region I, profiles are steepened, Ω_Z doesn't achieve the resonance condition, and non-resonant transport is dominant.*

In order to further understand the physical process behind this profile patterning, we need to discuss the flow evolution, since the resonant transport switch on depends sensitively on the value of Ω_Z. So we start from the evolution equation for mean vorticity $\overline{\Delta}\phi_Z$, i.e. Eq.(60). We can integrate it and explicitly include the effects of boundary conditions:

$$\begin{aligned}&\int_{x_1}^{x_2}\frac{\partial}{\partial t}\left(\delta_b^2\frac{\partial^2}{\partial x^2}\phi_Z\right)\mathrm{d}x = -\frac{1}{C_i}\int_{x_1}^{x_2}\frac{\partial}{\partial x}\left(\vartheta\chi^{\mathrm{n}}\frac{\partial}{\partial x}\frac{\ln\langle T\rangle}{\sqrt{2\varepsilon_0}}\right)\mathrm{d}x\\ &\quad+\frac{1}{C_i}\int_{x_1}^{x_2}\frac{\partial}{\partial x}\left(\vartheta\chi\delta_b^2\frac{\partial^3}{\partial x^3}\phi_Z\right)\mathrm{d}x + \int_{x_1}^{x_2}\nu_c\frac{\partial^2}{\partial x^2}\overline{\Delta}\phi_Z\mathrm{d}x\\ &\Longrightarrow \frac{\partial}{\partial t}\left(\delta_b^2\Omega_Z\right)\Big|_{x_1}^{x_2} = -\left(\frac{1}{C_i}\vartheta\chi^{\mathrm{n}}\frac{\partial}{\partial x}\frac{\ln\langle T\rangle}{\sqrt{2\varepsilon_0}}\right)\Big|_{x_1}^{x_2}\\ &\quad+\left(\frac{1}{C_i}\vartheta\chi\delta_b^2\frac{\partial^2}{\partial x^2}\Omega_Z\right)\Big|_{x_1}^{x_2} + \left(\nu_c\delta_b^2\frac{\partial^2}{\partial x^2}\Omega_Z\right)\Big|_{x_1}^{x_2}\end{aligned}$$

Then we write down the formal evolution equation of Ω_Z below according to the above expression as Eq.(71), where the boundary conditions Eq.(62)-(65) are used.

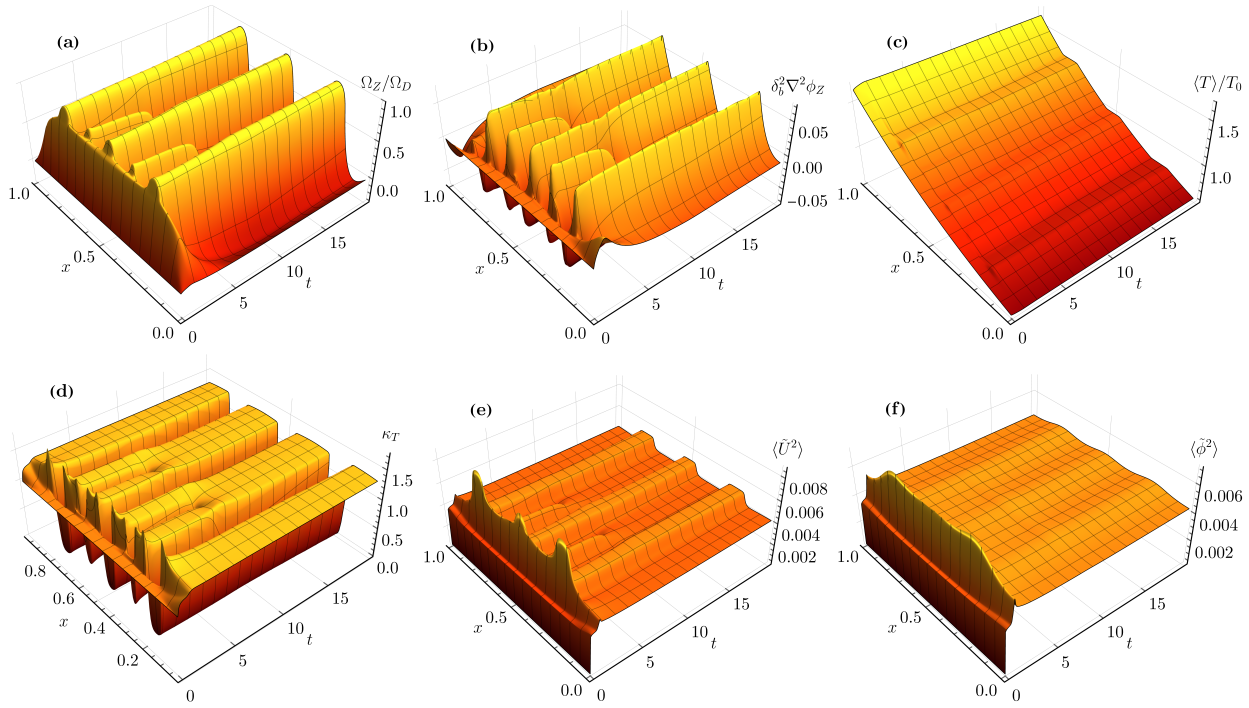

FIG. 5: Evolution of profiles from the system Eq.(60)-(68) with parameters in Tab. II. (a) $E\times B$ mean flow evolve a quasi-periodic structure in space. (b) Flow shear or mean vorticity profile evolution. (c) Temperature profile evolve a quasi-periodic staircase-like structure. (d) Temperature gradient profile. (e) Turbulence intensity evolution characterized by $\langle\tilde{U}^2\rangle$, which has clear corrugations in space. (f) Turbulence intensity evolution characterized by $\langle\tilde{\phi}^2\rangle$, in which corrugations are smoothed by Green's function Eq.(68).

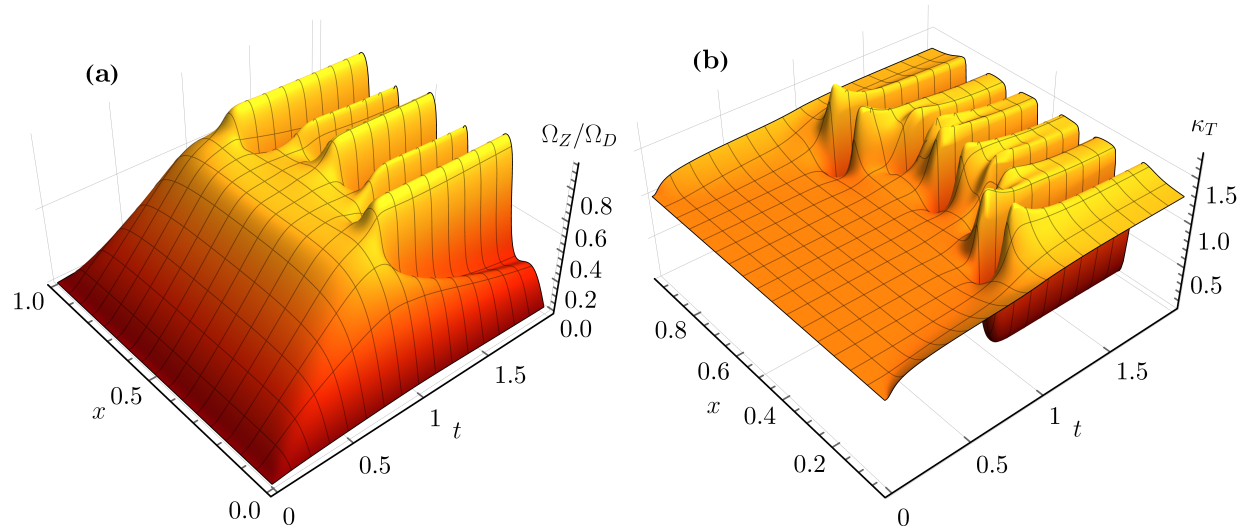

FIG. 6: Evolution of profiles (a) $E\times B$ mean flow and (b) temperature gradient in Figure 5 with extended time scale to show the onset of the pattern.

This can help us understand the staircase formation process.

$$\frac{\partial}{\partial t}\left(\delta_b^2\Omega_Z\right) = -\frac{1}{C_i}\vartheta\chi^{\mathrm{n}}\frac{\partial}{\partial x}\frac{\ln\langle T\rangle}{\sqrt{2\varepsilon_0}} + \frac{1}{C_i}\vartheta\chi^{\mathrm{n}}\frac{\partial}{\partial x}\frac{\ln\langle T\rangle}{\sqrt{2\varepsilon_0}}\bigg|_{\mathrm{B}} + \vartheta\chi\delta_b^2\frac{\partial^2}{\partial x^2}\Omega_Z + \nu_c\delta_b^2\frac{\partial^2}{\partial x^2}\Omega_Z \tag{71}$$

TABLE I: Definitions of quantities in Eq.(60)-Eq.(66)

Quantity	Definition
Ω_D	Trapped ion precession velocity
Ω_Z	$E\times B$ mean flow velocity
ϕ_Z	Mean electric potential
$\langle T\rangle$	Mean temperature
$\langle \tilde{U}^2\rangle$	Turbulence intensity
$\langle \tilde{\phi}^2\rangle$	Fluctuation electric potential intensity
C_i	$\omega_0 L_\psi q_i/T_i$
ε_0	Inverse aspect ratio a/R
ϑ	Parameter in transport coefficient model, <1
δ_b	Banana orbit width

TABLE II: Parameters for numerical solving Eq.(60)-Eq.(66)

Parameters	ϵ_0	τ	C_i	ρ_i	δ_b	Ω_D	ϑ	ν_c	$\chi_{\rm neo}$	$\nu_{\rm NL}$	$\kappa_T^{\rm I}$	$\Delta\kappa_T$
Values	1/4	1	0.1	10^{-2}	0.06	1	0.2	$0.1\chi^{\rm n}\delta_b^2$	$0.5\chi^{\rm n}\delta_b^2$	40	1	0.3

There is a clear drive of Ω_Z from the boundary temperature gradient in Eq.(71), i.e. the second term in the R.H.S. *Such drive will always exist, since we have set the boundary temperature gradient $\kappa_T^{\rm B}$ as fixed.* Because ν_c is small and $\Omega_Z|_{\rm B}=0$, to balance such constant drive and to let Ω_Z be quasi-steady, there are only two possibilities, as shown in FIG. 8.

- One is balance with the local temperature gradient, i.e. the first term in the R.H.S. of Eq.(71).
- Another is balance with the turbulent diffusion of Ω_Z itself, i.e. the third term in the R.H.S. of Eq.(71).

The different balances lead to different mean profile states. Different spatial locations can reach different balances, and therefore lead to different profile states.

Here, we explain the two states and the feedback loops to achieve them.

- In region I, we have the usual turbulent transport state with finite profile gradients. In this state, since $C_i\sqrt{2\varepsilon_0}\ll 1$ and $\partial_x\ln\langle T\rangle \gg C_i\sqrt{2\varepsilon_0}\partial_x\overline{\Delta}\phi_Z$, the vorticity gradient contribution can be neglected. The temperature gradient plays the central role in Eq.(71). Of course, the temperature profile is also determined in part by the boundary gradient $\kappa_T^{\rm B}$. More specifically, the local temperature gradient grows toward the boundary value in a typical time $\tau_{\nabla T}$ (defined in Eq.(76)). This process can be expressed formally as (assuming no initial gradient):

$$\partial_x\ln\langle T\rangle|_{(t,x)}\sim\left(1-e^{-t/\tau_{\nabla T}}\right)\partial_x\ln\langle T\rangle|_{\rm B}$$

Then, the final local temperature gradient almost reaches the boundary value. After this, in the flow evolution Eq.(71) , the residual difference between the $\kappa_T^{\rm B}$ and $\kappa_T^{\rm Local}$ is balanced through non-resonant turbulent transport and collisional dissipation of Ω_Z. Finally, Ω_Z will reach a quasi-steady state by balance between local and boundary temperature gradient, as illustrated in FIG. 8. In conclusion, the system will reach this state for which $\Omega_Z/\Omega_D<1$, which has finite gradients in both the temperature profile and the mean vorticity profile.

- In region II, we have the resonant transport state, with near flattened profiles. The detailed feedback loop to reach this state is shown in FIG. 9. As the flow Ω_Z grows, if it exceeds the resonance threshold, i.e. $\Omega_Z\gtrsim\Omega_D$, resonant transport is triggered. From Eq.(60) and Eq.(61), we know that the resonant transport appears in both equations. Both local temperature and mean vorticity transport are strongly enhanced by resonance. Therefore the local temperature gradient is flattened to a near-marginal state, as we hypothesized in section IV D. Recall that in the mean vorticity and mean flow evolution equation, the contribution from local thermal transport is purely non-resonant, and the local temperature gradient is small. The constant boundary temperature gradient drive in the Ω_Z evolution Eq.(71) cannot be balanced by the local temperature gradient, but rather through the enhanced (resonant) turbulent vorticity transport, as indicated in FIG. 8 and FIG. 9. In conclusion, the system will reach a state when $1<\Omega_Z/\Omega_D<1.5$,

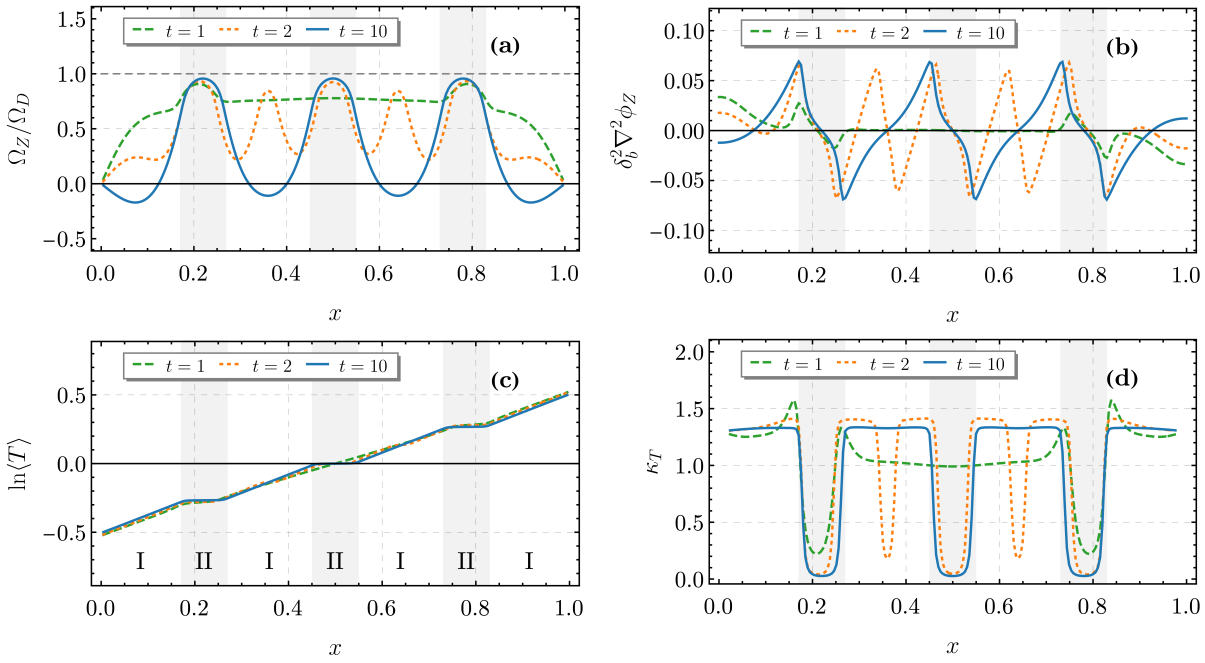

FIG. 7: Time slices of profiles. We named the regions with flatter temperature profiles the type II regions, regions with steeper temperature profiles the type I regions as in (c). (a) in type II regions, $E\times B$ mean flow profile satisfy the resonance condition $\Omega_D/\Omega_Z \gtrsim 1$, resonant transport is triggered. In type I regions, non-resonant transport is dominant. (b) is the slices of mean vorticity evolution. (d) is the slices of temperature gradient, where $\kappa_T \equiv \partial_x \ln\langle T\rangle$.

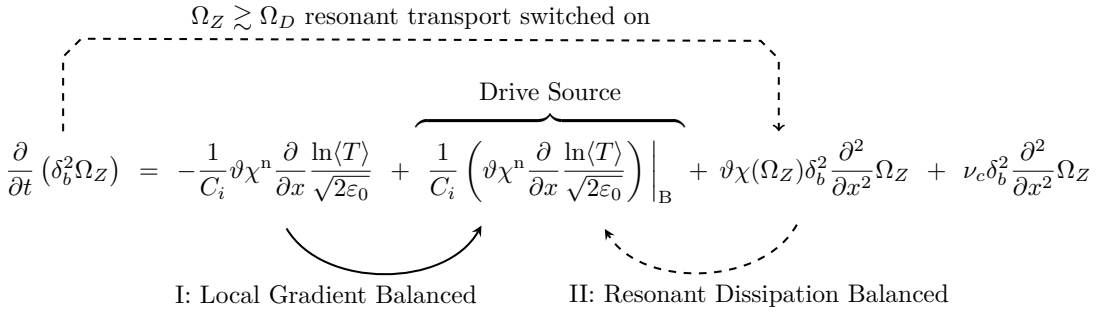

FIG. 8: Different scenarios of balancing with the boundary temperature drive in the formal evolution equation of Ω_Z. Either through I: growing local temperature gradient, or II: resonant diffusion of Ω_Z.

which has the marginal temperature profile and a less steep vorticity profile.

When profiles in a domain enter the type II feedback loop, the heat flux will be very strong and transport will exceed that for the neighboring domains. Therefore the κ_T in neighboring domains will increase (as shown in FIG.5(d)), and so the neighboring domains will be forced switch to the type I feedback loop. Thus, as long as resonant transport be triggered, the staircase pattern forms spontaneously.

With the above understanding of the feedback loops of two states, we can summarize the mechanism for staircase formation in a short story: *In addition to the usual non-resonant fluid-like turbulent transport, resonant transport leads to another possible state in both the temperature and vorticity profiles. The two transport-dominant states spontaneously form layers in space. Therefore a staircase involving resonant transport is formed.* The staircase pattern formation mechanism in this paper is different from those of former studies [6, 9, 24, 33, 58].

In the above story, one question still needs to be addressed: when will the staircase actually emerge? The answer is buried in the aforementioned feedback loops FIG. 9. We will uncover it in the following subsection.

C. Conditions for staircases to exist

From the previous discussion, we know to initiate feedback loop II – the most crucial step is the triggering the resonance condition, as shown in FIG. 8. Additionally,

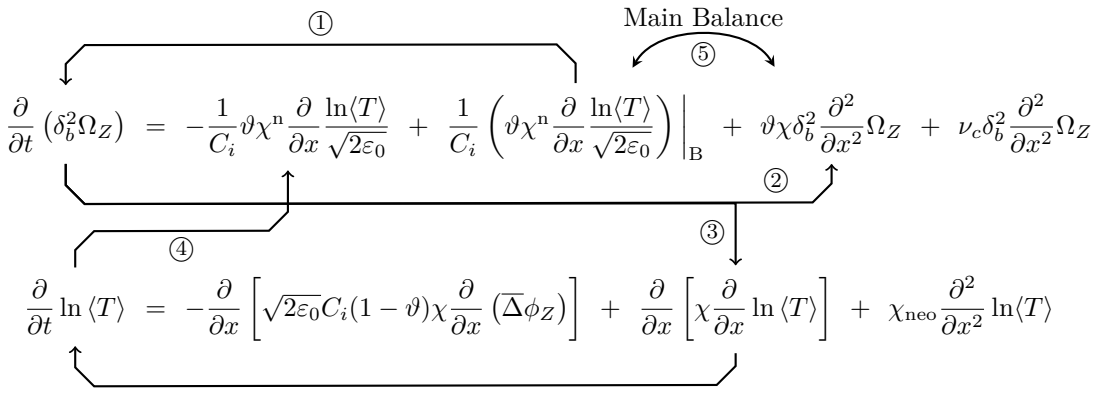

FIG. 9: Detailed feedback loop in type II Regions. ① Initially, the boundary value $\partial_x \ln\langle T\rangle|_{\rm B}$ is larger than the local value, which drives Ω_Z growing in the positive direction (since the boundary value is positive). If $\Omega_Z \gtrsim \Omega_D$, resonant transport $\chi^{\rm r}$ is switched on, ② diffusion of flow and ③ diffusion of local temperature are enhanced. ④ The local temperature profile is *flattened* and feeds back on the evolution of Ω_Z. Boundary temperature gradient effects become more significant since the local gradient is getting weaker. ⑤ The enhanced diffusion of Ω_Z at step ② can balance such an increase of drive. Eventually, Ω_Z reaches a quasi-steady state.

triggering must occur before the boundary temperature gradient drive is balanced by the local gradient, as shown in FIG. 9. Since both the local temperature gradient and the mean flow are driven by the boundary gradient $\kappa_T^{\rm B}$, the key for resonant transport to be switched on is *the time scale for Ω_Z to the resonance condition must be smaller than for the local κ_T to balance $\kappa_T^{\rm B}$*. Based on this simple logic, we will give an estimate of the threshold condition for staircase formation.

Let's start with a simple diffusion system like below, which has a constant diffusion coefficient:

$$\frac{\partial w}{\partial t} = a\frac{\partial^2}{\partial r^2}w + \Phi(r,t) \tag{72}$$

$$w_r\Big|_{r=0} = w_r\Big|_{r=l} = q_0 \tag{73}$$

$$w\Big|_{t=0} = f(r), \quad 0 \le r \le l \tag{74}$$

The analytical solution $w(r,t)$ can be obtained [59]. Then its gradient can be written as:

$$\begin{aligned}\frac{\partial w(r,t)}{\partial r} = &-\frac{2}{l^2}\int_0^l\int_0^t\left[\sum_{m=1}^{\infty}\pi m\Phi(\xi,\tau)\cos\left(\frac{\pi m\xi}{l}\right)\right.\\ &\left.\times\sin\left(\frac{\pi mr}{l}\right)e^{-\frac{\pi^2 a m^2(t-\tau)}{l^2}}\right]d\tau\,d\xi\\ &-\frac{2}{l^2}\int_0^l\sum_{m=1}^{\infty}\pi m f(\xi)\cos\left(\frac{\pi m\xi}{l}\right)\sin\left(\frac{\pi mr}{l}\right)e^{-\frac{\pi^2 a m^2 t}{l^2}}d\xi\\ &+q_0\sum_{m=1,3,5,\ldots}^{\infty}\frac{4}{\pi m}\sin\left(\frac{\pi mr}{l}\right)\left(1-e^{-\frac{\pi^2 a m^2 t}{l^2}}\right)\end{aligned}$$

Retaining to our model for the temperature profile Eq.(61), *consider the case where resonant transport has not yet been triggered*. We can neglect other terms and only consider the influence of the boundary gradient drive. Then we apply the above conclusion from the simple system, and obtain the expression for the local temperature gradient below:

$$\begin{aligned}\frac{\partial\ln\langle T\rangle}{\partial x}\Big|_{(x,t)} &\sim \frac{\partial\ln\langle T\rangle}{\partial x}\Big|_{\rm B}\\ &\times\left[1-\sum_{m=1,3,\ldots}^{\infty}\frac{4}{\pi m}\sin(\pi mx)\exp\left(-\pi^2\chi^{\rm n}m^2t\right)\right]\end{aligned} \tag{75}$$

Here we recall that $x \equiv \psi/L_\psi$. The first part of the series contributes 1. This expression tells us that the local temperature gradient evolves to the boundary value in a time scale of order

$$\tau_{\nabla T} \sim \frac{1}{\pi^2\chi^{\rm n}m^2} \tag{76}$$

Putting the estimate of the local temperature gradient above, into the evolution equation for Ω_Z Eq.(71), and keeping only the temperature-gradient-related terms gives:

$$\begin{aligned}\frac{\partial}{\partial t}\Omega_Z &\sim \frac{1}{C_i}\frac{\vartheta\chi^{\rm n}}{\delta_b^2\sqrt{2\varepsilon_0}}\left[\frac{\partial}{\partial x}\ln\langle T\rangle\Big|_{\rm B} - \frac{\partial}{\partial x}\ln\langle T\rangle\Big|_{(x,t)}\right]\\ &= \frac{1}{C_i}\frac{\vartheta\chi^{\rm n}}{\delta_b^2\sqrt{2\varepsilon_0}}\frac{\partial\ln\langle T\rangle}{\partial x}\Big|_{\rm B}\\ &\quad\times\sum_{m=1,3,\ldots}^{\infty}\frac{4}{\pi m}\sin(\pi mx)\,e^{-\pi^2\chi^{\rm n}m^2t}\end{aligned} \tag{77}$$

This gives the evolution of Ω_Z driven by the boundary

heat flux, before resonant transport is triggered. Thus:

$$\Omega_Z(t,x) \sim \frac{1}{C_i}\frac{\vartheta\chi^{\rm n}}{\delta_b^2\sqrt{2\varepsilon_0}}\frac{\partial\ln\langle T\rangle}{\partial x}\bigg|_{\rm B}\sum_{m=1,3,\dots}^{\infty}\left[\frac{4}{\pi m}\sin(\pi m x)\right.$$
$$\left.\times\,\tau_{\nabla T}\left(1-e^{-\pi^2\chi^{\rm n}m^2 t}\right)\right] \tag{78}$$

Recall the key for the switch-on of resonant transport is for Ω_Z *to reach the resonance condition* $\Omega_Z \geq \Omega_D$ *before the local temperature gradient equals the boundary gradient.* The time scale for the local temperature gradient to become comparable to the boundary value is $\tau_{\nabla T}$ as shown in Eq.(75). So the condition is equivalent to saying there is $\Omega_Z(\tau_{\nabla T},x) > \Omega_D$, at $t=\tau_{\nabla T}$:

$$\Omega_Z(\tau_{\nabla T},x) \sim \frac{1}{C_i}\frac{\vartheta}{\delta_b^2\sqrt{2\varepsilon_0}}\frac{\partial\ln\langle T\rangle}{\partial x}\bigg|_{\rm B}$$
$$\times\sum_{m=1,3,\dots}^{\infty}\frac{4}{(\pi m)^3}\sin(\pi m x)\left(1-\frac{1}{e}\right) \tag{79}$$
$$> \Omega_D$$

This gives the requirement for the boundary temperature gradient scale length:

$$\frac{\partial\ln\langle T\rangle}{\partial x}\bigg|_{\rm B} > \frac{eC_i\Omega_D\delta_b^2\sqrt{2\varepsilon_0}}{(e-1)\vartheta\sum_{m=1,3,\dots}^{\infty}\frac{4\sin(\pi m x)}{(\pi m)^3}} \tag{80}$$

The series in the dominator above is a function of $x\in[0,1]$, which has the value domain of $[0,0.125]$, with the maximum value at $x=0.5$. As we mentioned in the previous subsection that *as long as resonance transport be triggered, the staircase pattern forms spontaneously.* So the trigger sign we are looking for is that any position in space is satisfied the resonance condition. Thus we take the maximum value of the series. We also set the factor $e/(e-1)\sim 1$ for simplicity. Then we can write the threshold for the resonant transport to switch on as:

$$\frac{\partial\ln\langle T\rangle}{\partial x}\bigg|_{\rm B} > C_i\Omega_D\frac{8\delta_b^2\sqrt{2\varepsilon_0}}{\vartheta} \tag{81}$$

This is the threshold for the initial value of $\partial_x\ln\langle T\rangle = 0$. Restoring the initial condition effect gives us the threshold:

$$\Delta\kappa_T^{\rm crit} \equiv \frac{\partial\ln\langle T\rangle}{\partial x}\bigg|_{\rm B} - \frac{\partial\ln\langle T\rangle}{\partial x}\bigg|_{\rm I} > C_i\Omega_D\frac{8\delta_b^2\sqrt{2\varepsilon_0}}{\vartheta} \tag{82}$$

Because of $x=\psi/L_\psi$, $L_\psi=-B_\theta R_0 a$ and $\mathrm{d}\psi = -B_\theta R_0\mathrm{d}r$, we have $\mathrm{d}x=\mathrm{d}r/a$. Meanwhile, there is $C_i = q\omega_0 L_\psi/T_i$. We also restore Ω_D and δ_b to the forms before simplification as $\Omega_D T_0/\omega_0$ and δ_b/a. Then the threshold Eq.(82) can be written in the minor radius coordinate as:

$$\frac{1}{L_T}\bigg|_{\rm B} - \frac{1}{L_T}\bigg|_{\rm I} < -\frac{q}{T_0}\Omega_D T_0 B_\theta R_0\left(\frac{\delta_b}{a}\right)^2\frac{8\sqrt{2\varepsilon_0}}{\vartheta} \tag{83}$$

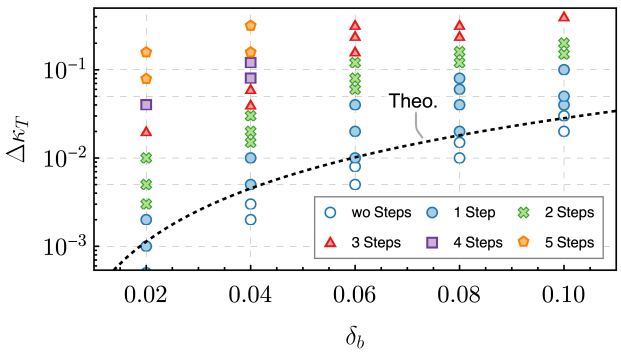

FIG. 10: Scan of $\Delta\kappa_T^{\rm crit}$ by varying δ_b and $\Delta\kappa_T$ with $\kappa_T^{\rm I}=1$. Different markers represent the number of steps observed. When boundary drive exceeds a threshold (from hollow circles to filled circles), step (plateau) will form. The analytical prediction from Eq.(82) is plotted as the dotted line, which well fits with the numerical scan of the threshold. Larger boundary drive ($\Delta\kappa_T$) results in more steps. Smaller δ_b leads to more steps.

Noticing $\Omega_D T_0$ is the the precession velocity of trapped ions in α direction, so the unit of it is rad per second. With $\Omega_D \propto q_s(r_0)/(qr_0R_0B_0)$ and safety factor $q_s(r_0) = r_0B_0/(R_0B_\theta)$ [60], we then have:

$$\frac{1}{L_T}\bigg|_{\rm B} - \frac{1}{L_T}\bigg|_{\rm I} < -\frac{8\sqrt{2}}{\vartheta}\frac{1}{R_0}\sqrt{\frac{a}{R_0}}\left(\frac{\delta_b}{a}\right)^2 \tag{84}$$

To validate the estimate we obtained, we scan the system by varying parameters. For instance, for $C_i = 0.1, \Omega_D = 1, \varepsilon_0 = 1/4, \vartheta = 0.2$, we vary δ_b from 0.02 to 0.1. We set $\kappa_T^{\rm I} \equiv \partial_x\ln\langle T\rangle|_{\rm I} = 1$ and scan $\kappa_T^{\rm B} \equiv \partial_x\ln\langle T\rangle|_{\rm B} = \kappa_T^{\rm I} + \Delta\kappa_T$ to obtain FIG. 10. The different markers represent the number of steps observed. Stronger flux drive leads to more steps. The threshold Eq.(82) from the simple theoretical prediction is plotted as the dotted line, which captures the actual $\Delta\kappa_T$ threshold from numerical scans of the system. But we need to keep in mind that Eq.(82) does not include the $\chi_{\rm neo}$ and ν_c effects, which can play more important roles when $\Delta\kappa_T$ is near threshold. And for the purpose of smooth calculation, there is a "bandwidth" around $\Omega_Z=\Omega_D$ in the transport coefficient model in FIG.2, which can affect the threshold too.

D. Features of staircases

From the evolution of Ω_Z Eq.(71), we know that in region II, to maintain a quasi-steady Ω_Z, there should be a balance of boundary heat flux drive and local resonant transport of Ω_Z:

$$\left(\frac{1}{C_i}\chi^{\rm n}\frac{\partial}{\partial x}\frac{\ln\langle T\rangle}{\sqrt{2\varepsilon_0}}\right)\bigg|_{\rm B} \sim \chi^{\rm r}\delta_b^2\frac{\partial^2}{\partial x^2}\Omega_Z \tag{85}$$

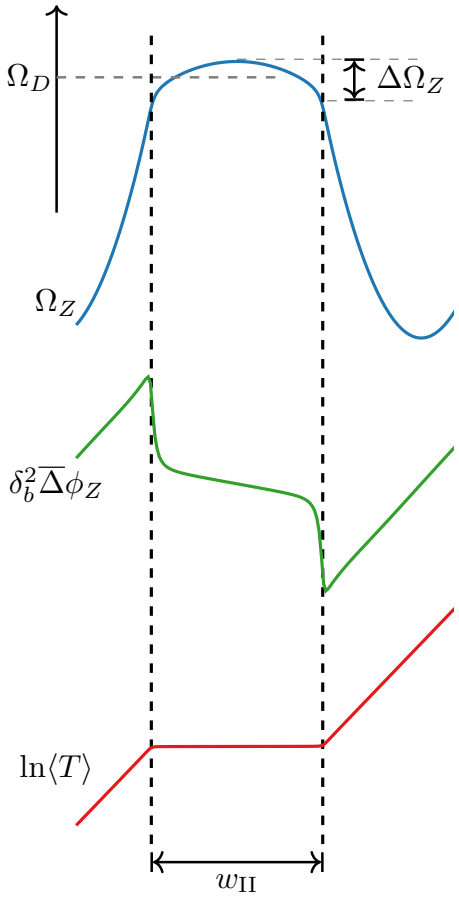

FIG. 11: A diagram for profiles. Flow Ω_Z that are at resonance and the width of plateau region $w_{\rm II}$ correspond.

Because in the L.H.S. of the relation above, $\partial_x \ln\langle T\rangle|_{\rm B}$ is a constant, the Ω_Z in Region II should be in the form of a quadratic function:

$$\Omega_Z(x) \to -K_{\rm II}x^2 \tag{86}$$

where $K_{\rm II}$ is a parameter. Putting this form of Ω_Z into the balance relation Eq.(85) gives:

$$K_{\rm II} \sim \frac{1}{\delta_b^2 C_i\sqrt{2\varepsilon_0}}\frac{\chi^{\rm n}}{\chi^{\rm r}}\left(\frac{\partial \ln\langle T\rangle}{\partial x}\right)\Big|_{\rm B} \tag{87}$$

Recall the model of $\chi(\Omega_Z)$ in FIG. 2. In the half width of the plateau region width $w_{\rm II}$, Ω_Z should decrease from the maximum value $\Omega_Z^{\rm Max}$ to the minimum value that can trigger resonant transport $\Omega_Z^{\rm Crit}$, as illustrated in FIG. 11. The difference between the maximum and minimum values is defined as $\Delta\Omega_Z$ here. Then from FIG. 11 and Eq.(86), we have that the variation of Ω_Z in the spatial range of $w_{\rm II}/2$ equals $\Delta\Omega_Z$:

$$K_{\rm II}\left(\frac{w_{\rm II}}{2}\right)^2 \sim \Omega_Z^{\rm Max} - \Omega_Z^{\rm Crit} \equiv \Delta\Omega_Z$$

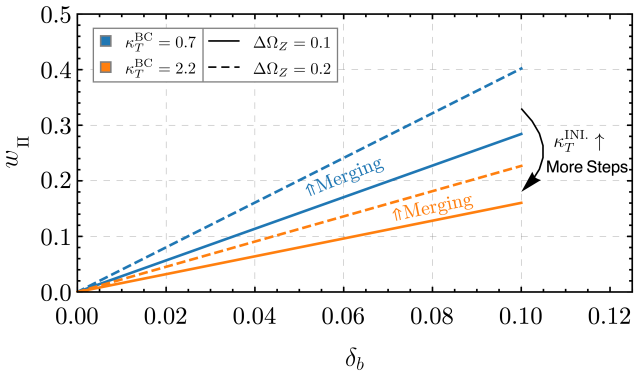

FIG. 12: The plateau width v.s. δ_b, with different $\Delta\Omega_Z$ and $\kappa_T^{\rm B}$ according to Eq.(88). Here $\kappa_T^{\rm B}=\kappa_T^{\rm I}+\Delta\kappa_T$. (a) With the same boundary drive, for example $\Delta\kappa_T=0.2$, a bigger initial temperature gradient can lead to a smaller step size, therefore a larger number of steps is possible. (b) For a set of $(\delta_b,\kappa_T^{\rm B})$, as the flow slightly grows, $\Delta\Omega_Z$ will slightly grow, for example from 0.1 to 0.2. This is manifested as the merging of steps.

Here $\Delta\Omega_Z$ is related to the "bandwidth" w_Ω that we defined in the χ model in FIG. 2. Therefore combining the expression for $K_{\rm II}$ in Eq.(87), we obtain the estimate of the plateau or step width as:

$$w_{\rm II} \sim 2\sqrt{\frac{\Delta\Omega_Z}{K_{\rm II}}} \sim 2\delta_b\sqrt{\Delta\Omega_Z\frac{\chi^{\rm r}}{\chi^{\rm n}}\frac{C_i\sqrt{2\varepsilon_0}}{\partial_x\ln\langle T\rangle|_{\rm B}}} \tag{88}$$

For example, we take $\chi/\chi^{\rm n}=100$, $C_i=0.1,\varepsilon_0=1/4$, and $w_\Omega=0.2\sim\Delta\Omega_Z/\Omega_D$ from the $\chi(\Omega_Z)$ model. Then the relation (Eq.(88)) between $w_{\rm II}$ and δ_b can be plotted for different $\Delta\kappa_T$ as in FIG. 12. From the numerical results, we find that after $\Omega_Z\simeq\Omega_D$, Ω_Z may still grow slowly, therefore $\Delta\Omega_Z$ also grows slowly. Then the typical size of the plateau region also increases slightly. Since the maximum step number is limited by $1/w_{\rm II}$, a decreasing in $1/w_{\rm II}$ is manifested as the merging of steps, as illustrated in FIG. 12.

In FIG. 13, we use the same $\Delta\kappa_T$, but change the initial value $\kappa_T^{\rm I}$. The results show that a larger initial gradient decreases the plateau width and allow more steps to exist, just as Eq.(88) predicted. But after changing $\kappa_T^{\rm I}$, if we want to maintain the extra steps, we need a stronger $\Delta\kappa_T$. Otherwise, the steps will merge, as in FIG. 13II. For more complicated initial profiles-other than with a constant gradient-the locations of pattern and step number can change.

In conclusion, the step size is proportional to the banana width and is heavily influenced by the ratio of resonant to non-resonant transport coefficients. The total temperature gradient (or heat flux, since χ is always non-resonant at the boundaries) at the boundaries $\kappa_T^{\rm B}=\kappa_T^{\rm I}+\Delta\kappa_T$ determines the typical width of the plateau (steps) in the $E\times B$ staircase, and therefore limits the maximum possible number of steps. The steps that

actually appear and maintain are determined by the "free energy" that passes through the system, i.e.the increment of heat flux $\chi^{\rm n}\Delta\kappa_T$. Therefore, larger $\Delta\kappa_T$ allows more steps to form. *The stronger the net drive $\Delta\kappa_T$ is, the greater the number of steps.*

VI. DISCUSSION AND CONCLUSIONS

In this paper, we studied mean profile evolution in a potential vorticity conserving system for ITG-driven trapped ion mode turbulence, which is derived from the Darmet model. The Darmet model is perhaps the simplest possible gyro-kinetic drift wave model, and exhibits many generic properties. We use the quasi-linear approximation to establish the relation between the heat flux, vorticity flux, potential vorticity flux and the profiles of mean temperature and mean vorticity. The mean profile evolution equations are closed by these flux-gradient relations. We also include the extended turbulence intensity evolution equation for potential enstrophy $\langle\tilde{U}^2\rangle$, and then transform from $\langle\tilde{U}^2\rangle$ to $\langle\tilde{\phi}^2\rangle$ using a Green's function. Taken together, these equations constitute a turbulence and profile evolution system. In this system, trapped ions can resonate with the (trapped ion) mode through a Doppler shift due to $E\times B$ toroidal mean flow. Such resonance between wave and particle leads to resonant transport. Spatial variation in the flow profile then necessarily leads to variation in the balance of resonant and non-resonant transport.

We use the dispersion relation obtained from the Darmet system and a bi-Lorentzian spectrum model to simplify the transport coefficients appearing in the fluxes. We obtain three important conclusions:

1. The resonance condition can be directly linked to a requirement on the $E\times B$ mean flow, i.e. $1\lesssim\Omega_Z/\Omega_D\lesssim 1.5$.

2. The ratio between resonant and non-resonant transport coefficients is approximately: $\chi^{\rm r}/\chi^{\rm n}\sim(\omega_R/\gamma)^2\sim\mathcal{O}(10)-\mathcal{O}(100)$. Here the square relation is a result of the calculating of the Lorentzian spectrum with the TIM dispersion relation.

3. All the transport effects are condensed into coefficients, so we can simplify them with a unified model.

Based on these conclusions, we model the transport coefficients as piecewise functions of Ω_Z, and simplify the system. Then combining the profile evolution equation, the turbulence intensity evolution equation, the boundary conditions and the transport coefficient model, we finally obtain a solvable turbulence-profile evolution system which contains resonant and non-resonant turbulent transport, as Eq.(60)-(66). We use this system to study the profile evolution and $E\times B$ staircase formation.

We solve this turbulence-profile evolution system with a fixed boundary flux drive $\kappa_T^{\rm B}\equiv\partial_x\ln\langle T\rangle|_{\rm B}$. The results show that when boundary drive $\kappa_T^{\rm B}-\kappa_T^{\rm I}$ is strong enough (where $\kappa_T^{\rm I}\equiv\partial_x\ln\langle T\rangle|_{(x,t=0)}$), the profiles will evolve into a $E\times B$ staircase, which is a quasi-periodic pattern in temperature gradient and $E\times B$ mean flow shear. According to the states of the temperature profile, we categorize the structures which occur in two regions.

- In the corrugation region (Region I), non-resonant turbulent transport is dominant and temperature profiles are steeper. The profiles of mean flow and mean vorticity are determined by the remnants of boundary gradient drive, non-resonant turbulent diffusion and collisional dissipation of mean flow itself.

- In the plateau regions (Region II), where mean flow has values near precession velocity Ω_D and induces resonant transport, the temperature profiles are near marginal and shallow. In the evolution of mean flow (or flow shear, mean vorticity), the main saturation mechanism is the resonant turbulence diffusion of flow itself.

Resonant and non-resonant transport regions are determined by the $E\times B$ mean flow profile, the structure of which forms spontaneously in space when resonant transport is triggered. The variation of turbulence intensity $\langle\tilde{\phi}^2\rangle$ between regions I and II is small, because the Green's function heavily smooths the corrugations or patterns in the profile of $\langle\tilde{U}^2\rangle$. So the $E\times B$ staircase pattern which emerges in this system is a result of the transition from non-resonant to resonant transport triggered by $E\times B$ mean flow structure, and not a result from the turbulence intensity variation in space. Of course, the $E\times B$ mean flow and thermal transport are generated from turbulence, so the turbulence still plays an essential role in the self-organized structure.

After studying the feedback loops of staircase formation, we conclude the condition for the staircase pattern to form is for the boundary heat flux to be strong enough to drive the $E\times B$ mean flow sufficiently to satisfy the resonance condition prior to when the local temperature gradient equals the boundary value. Eq.(82) is the estimate of the required critical boundary temperature gradient derived from this condition. The staircase will be triggered when $\Delta\kappa_T>\Delta\kappa_T^{\rm crit}$. A scan of our turbulence-profile evolution system Eq.(60)-(66) shows that $\Delta\kappa_T^{\rm crit}$ constitutes the threshold criterion, as in FIG. 10.

For $E\times B$ mean flow Ω_Z to maintain a quasi-steady state, we need the constant boundary heat flux drive to balance with the local resonant turbulent transport of Ω_Z. According to this, we obtain an estimate of the step size of staircase pattern, Eq.(88). The step size is:

1. proportional to the banana orbit width δ_b;

2. proportional to $\sqrt{\chi^{\rm r}/\chi^{\rm n}}$. Since the ratio between resonant and non-resonant transport coefficients is

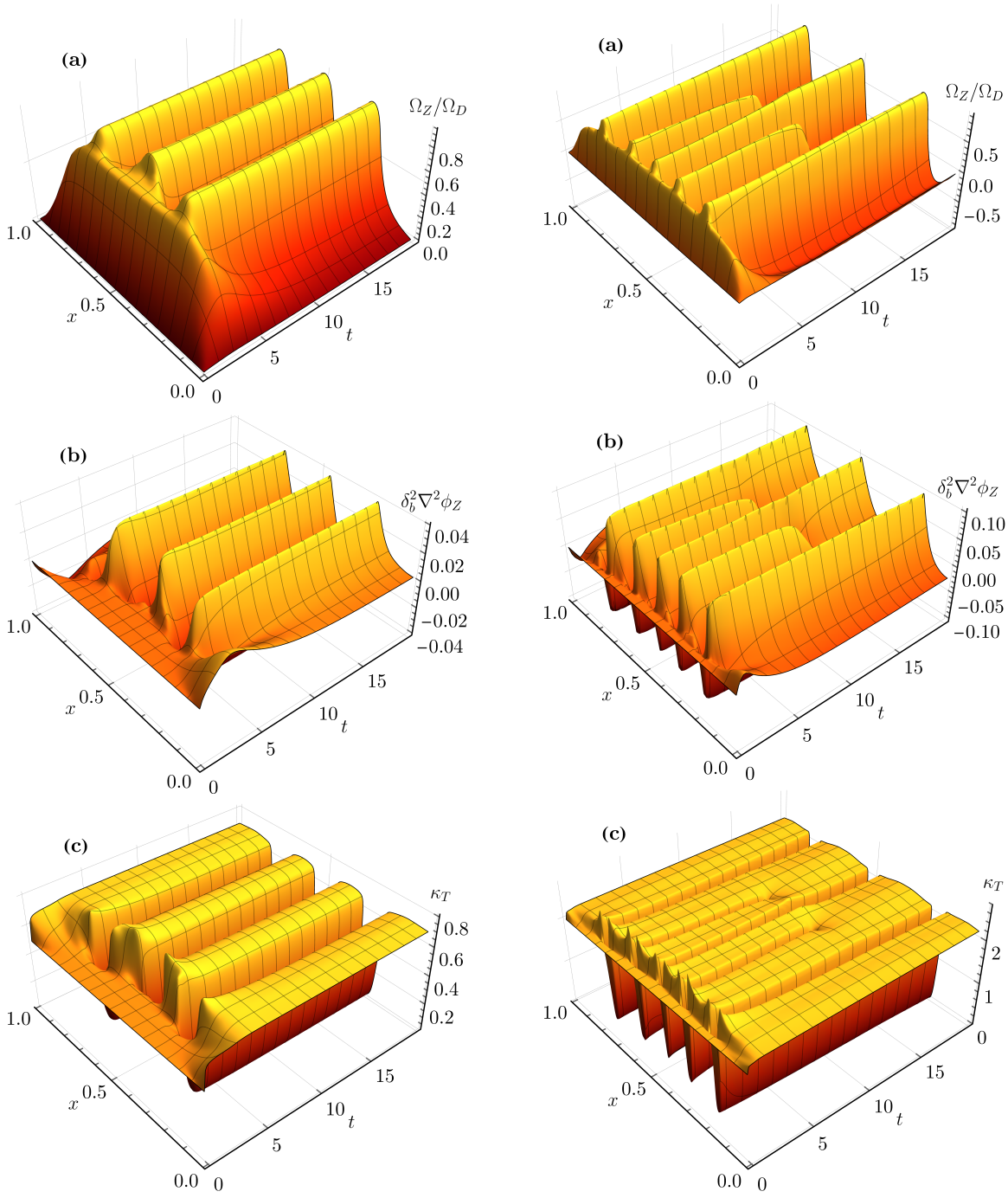

FIG. 13: The initial value of $\partial_x \ln\langle T\rangle$ can affect the step size and step number. With $\Delta\kappa_T = 0.2$, $\delta_b = 0.06$.

approximately the square of the ratio of the real frequency and the growth rate of TIM, the step size is proportional to $|\omega_R/\gamma| > 1$;

3. inversely proportional to $\sqrt{\kappa_T^{\mathrm{B}}}$, i.e. the stronger the boundary heat flux is, the narrower the steps are.

According to the third point above, increasing $\kappa_T^{\mathrm{B}} = \kappa_T^{\mathrm{I}} + \Delta\kappa_T$ decreases the step size, and therefore allows more steps in a finite domain. This is because a stronger heat flux drives the system evolution further towards the direction of enstrophy reduction (as indicated in Eq.(C8) shown in Appendix C), which corresponds to a more "regular" structure. But to make the pattern clearer and to maintain more steps, a strong net boundary drive $\Delta\kappa_T$

is necessary.

Many assumptions and approximations have been made in this work. The Darmet model we used is for trapped ion mode, in which the turbulence frequency is smaller than the bounce frequency. We dropped density evolution effects in the derivation of total PV $\langle q\rangle + \delta q$. $|q_i\phi/T| \ll 1$ is assumed as a small parameter. Quasi-linear approximation we used is effective when the Kubo number $Ku < 1$. Models of the dispersion relation are used. The bi-Lorentz spectrum model is used–indeed, this approximation has a major impact on the result. An approximate transport coefficient model is used to unify all transport coefficients in the quasi-linear flux. The triplet nonlinearity in turbulence intensity evolution equation is approximated with a diffusion effect and a nonlinear damping effect. These can be improved in the future. We made a hypothesis on the near marginality profile to address the issue of the flatten temperature profile relaxed by the resonant turbulent transport. All these approximations, assumptions and hypothesis limit our model. Most of them can be improved in future studies.

As we have stated at the beginning of this paper, the Darmet model applies to conditions of low turbulence frequency, low collisionality, etc. Then the question of how this model relates to the usual regimes where ITG and trapped electron mode (TEM) (regarded as the basic turbulence drives) are active is raised. First, we clarify that the Darmet model indeed applies for different conditions from the ITG/TEM, as usually discussed. But the Darmet is perhaps the simplest kinetic model for drift wave turbulence that manifests zonal flow, resonant particles, etc. Due to the simplicity of the Darmet model, we can easily construct a theory that contains the interplay between turbulence, mean flow, and wave-particle resonance, as we showed in this paper. And such interplay can generate a staircase-like pattern in profiles, which is an interesting self-organized structure. In a sense, the theory in this paper can be regarded as a kind of paradigm for self-organization and pattern formation in *kinetic* drift wave theory. Then, we can study whether there exist similar patterns in the usual ITG/TEM condition. Alternatively, for the condition of a higher fraction of trapped ion or fast ions, the question of whether the resonance mechanism helps improve confinement is interesting. Finally, it is still unknown whether the trapped ion mode makes significant contributions in the gyrokinetic simulations or experiments. We will continue to explore the limitations of our theory in the future.

In conclusion, this paper studied a turbulence-profile evolution system with resonant and non-resonant transport. This is a new realization of the general idea of inhomogeneous mixing and bistable transport[30]. We found the profile staircase pattern ($E\times B$ staircase) caused by the onset of resonant turbulent transport and analyzed the feedback mechanism which forms the pattern. We obtained an estimate of the trigger condition for $E\times B$ staircase formation and the estimate of the step size in the staircase. This work also provides a mechanism for collisionless saturation of the zonal flow, i.e. through the resonant turbulent zonal vorticity flux, as did in Ref.[61]. This work also has potential connection to the studies for ITB triggering by resonance between turbulence and particles [62, 63]. The existence of staircase also suggests some possible improved confinement scenarios, of an "enhanced L mode" type. We will continue to explore the potential applications of the theory of $E\times B$ staircase and resonance mechanism discussed in this paper, and especially applications to confinement improvement.

ACKNOWLEDGMENTS

This work is supported by National Key R&D Program of China under 2018YFE0303102, National Natural Science Foundation of China under Grant No. U186722, 11875124, 11905051, Science and Technology Department of Sichuan Province under Grant No. 2020JDTD0030. The work is also supported by the U.S. Department of Energy, Office of Science, Office of Fusion Energy Sciences under Award Number DE-FG02-04ER54738.

Appendix A: Dispersion function

For the kinetic system Eq.(4)-(5), the ordering of scales are,

$$\omega_{ti},\omega_{bi} > \omega^i_* > \omega \sim \omega_{Di} > \nu^i_{eff} \tag{A1}$$

$$\omega_{te},\omega_{be} > \nu^e_{eff} > \omega^e_* > \omega \tag{A2}$$

The quantities in the first set of relation are the transit frequency and bounce frequency of trapped ion, diamagnetic frequency, TIM frequency, magnetic drift frequency, and collision frequency for ions. The second set is for electrons. The kinetic equation and quasi-neutrality equation with normalized quantities are:

$$\begin{aligned}&\partial_t h_i + \Omega_D E\partial_y h_i - \left[\phi, -C_i\tilde{\phi}\langle f_i\rangle + h_i\right]\\ &= \partial_t\left(C_i\tilde{\phi}\langle f_i\rangle\right) + \partial_y(\overline{\phi - \langle\phi\rangle_y})\partial_\psi\langle f_i\rangle\end{aligned} \tag{A3}$$

$$C_{ad}\tilde{\phi} - C_i\overline{\Delta}\phi = \frac{2}{n_0\sqrt{\pi}}\int_0^\infty J_0 h_i\sqrt{E}\mathrm{d}E \tag{A4}$$

where $(\psi,\alpha)\to(x,y)$, h_i is the non-adiabatic fluctuation, and we already assumed adiabatic electrons. $\hat{\Omega}_D = \Omega_D T_0/\omega_0$, $\hat{E} = E/T_0$, $C_i = \omega_0 L_\psi q_i/T_0$, where " $\hat{}$ " are neglected here and after.

Applying Fourier transformation to the kinetic equation Eq.(A3), and dropping the zonal portion in ϕ and

the Poisson bracket, one obtains:

$$\begin{aligned}(-i\omega + ik_y\Omega_D E)h_i &= -i\omega C_i\tilde{\phi}\langle f_i\rangle + ik_y\tilde{\phi}\partial_x\langle f_i\rangle \\ &= -i\omega C_i\tilde{\phi}\langle f_i\rangle + \frac{ik_y}{C_i}\frac{\partial_x\langle f_i\rangle}{\langle f_i\rangle}C_i\tilde{\phi}\langle f_i\rangle \\ &= -i[\omega - \omega_*^i(E)]C_i\tilde{\phi}\langle f_i\rangle\end{aligned}$$

where,

$$\omega_*^i(E) = \frac{k_y}{C_i}\frac{\partial_x\langle f_i\rangle}{\langle f_i\rangle}$$

Then,

$$h_i = \frac{\omega - \omega_*^i(E)}{\omega - k_y\Omega_D E}C_i\tilde{\phi}\langle f_i\rangle \tag{A5}$$

Let,

$$z \equiv \frac{\omega}{k_y\Omega_D} \tag{A6}$$

$$\omega_*(E) \equiv \frac{\omega_*^i(E)}{k_y\Omega_D} = \frac{1}{C_i\Omega_D}\left[\kappa_n + \kappa_T\left(E - \frac{3}{2}\right)\right] \tag{A7}$$

Assuming $\langle f\rangle_i = n_0 e^{-E}$, then we have:

$$h_i = \frac{z - \omega_*(E)}{z - E}C_i\tilde{\phi}n_0 e^{-E} \tag{A8}$$

For the interchange-like mode of TIM, the dispersion function can be obtained by putting the expression of h_i above into Eq.(A4) and directly integrating it with E. Notice z is assumed to be a complex number here. Now we obtain the dispersion function for TIM:

$$\begin{aligned}D(k,\omega) &= (C_{ad}/C_i) + \rho_{i0}^2k_y^2 + \delta_{b0}^2k_x^2 \\ &\quad - \frac{2}{\sqrt{\pi}}\int_0^\infty \frac{z - \omega_*(E)}{z - E}e^{-E}\sqrt{E}\mathrm{d}E \qquad \text{(A9)} \\ &= (C_{ad}/C_i) + \rho_{i0}^2k_y^2 + \delta_{b0}^2k_x^2 \\ &\quad + 2\left[z - \frac{\kappa_n}{C_i\Omega_D}\left(1 - \frac{3\eta_i}{2}\right)\right] \\ &\quad \times \left[1 - \sqrt{\pi}e^{-z}\sqrt{-z} - 2\sqrt{z}F\left(\sqrt{z}\right)\right] \\ &\quad - \frac{\kappa_T}{C_i\Omega_D}\left[1 + 2\left(\sqrt{\pi}e^{-z}(-z)^{3/2} + z\right)\right. \\ &\quad \left. - 4z^{3/2}F\left(\sqrt{z}\right)\right] \qquad \text{(A10)}\end{aligned}$$

where $F(x)$ is the Dawson integral:

$$F(x) = e^{-x^2}\int_0^x e^{y^2}\mathrm{d}y \tag{A11}$$

Using the plasma dispersion function Z_p, we can write the dispersion function as:

$$\begin{aligned}D(k,z) &= (C_{ad}/C_i) + \rho_{i0}^2k_y^2 + \delta_{b0}^2k_x^2 \\ &\quad + 2\left[z - \frac{\kappa_n}{C_i\Omega_D}(1 - \frac{3\eta_i}{2})\right]\left[1 + \sqrt{z}Z_p(\sqrt{z})\right] \\ &\quad - \frac{\kappa_T}{C_i\Omega_D}\left[1 + 2z + 2z^{3/2}Z_p(\sqrt{z})\right] \qquad \text{(A12)}\end{aligned}$$

1. The linear instability threshold κ_T^c

Following the usual Landau's prescription, there are real and imaginary contributions in Eq.(A12). In the case of marginal growth rate, where $\gamma \simeq 0$, the marginal real frequency must keep the imaginary part of dispersion function to be 0, i.e. $\Im D(k,\omega_{\rm th}) = 0$. This corresponds to:

$$\Im D(k,\omega_{\rm th}) = 0 \Rightarrow z - \omega_*(E_{\rm res}) = 0$$

where $E_{\rm res} = \omega/(k_y\Omega_D)$. It's easy to obtain the marginal real frequency from the expression above:

$$\omega_{\rm th} = \frac{\kappa_n - \frac{3}{2}\kappa_T}{C_i\Omega_D - \kappa_T}k_y\Omega_D \tag{A13}$$

Putting $\omega_{\rm th}$ into the real part of $D(k,\omega_{\rm th}/(k_y\Omega_D))$ and letting it be 0, this gives the critical threshold for κ_T (where κ_n are assumed to be 0 in this paper) as:

$$\kappa_T^c = C_i\Omega_D\left[C_{ad}/C_i + \left(\rho_{i0}^2k_y^2 + \delta_{b0}^2k_x^2\right)\right] \tag{A14}$$

Only when the local temperature gradient is larger than κ_T^c, can the linear instability be excited. Besides, Eq.(A14) also provides a limitation for wave numbers:

$$\Theta_{\rm max} \equiv \rho_i^2k_{y,\rm max}^2 + \delta_b^2k_{x,\rm max}^2 = \frac{\kappa_T}{C_i\Omega_D} - \frac{1+\tau}{\sqrt{2\varepsilon_0}} \tag{A15}$$

When the parameters in the R.H.S of Eq.(A15) take ϵ_0, τ, C_i in Table III, and $\Omega_D = 1$, $\kappa_T = 0.4$, we will have $\Theta_{\rm max} \simeq 1.17$. Eq.(A15) can well fit the numerical result in FIG. 14. κ_T and other parameters in criterion Eq.(A15) can affect the value of $\Theta_{\rm max}$. But as long as parameters are around the values in Table III, we will always have $\Theta_{\rm max} \sim \mathcal{O}(1)$. So for simplicity, we just take $\Theta_{\rm max} \sim 1$ and use it in the calculation of transport coefficients in section IV.

2. Real frequency and growth rate

When the parameters in dispersion function Eq.(A12) take the values in Table III, we can numerically calculate the dispersion relation, the results are shown in FIG. 15. The real frequency can be well fit by the relation

$$\omega_R = \frac{R_1k_y\Omega_D}{1 + R_2(\rho_i^2k_y^2 + \delta_b^2k_x^2)} \tag{A16}$$

where $R_1 \simeq 2.3675, R_2 \simeq 0.16 \ll 1$. So there is $\omega_R \simeq Rk_y\omega_D = 2.36k_y\omega_D$. Such a model for the real frequency is effective for moderately varying κ_T as shown in FIG. 15(a). Notice the factor R is different from the results in Ref.[34, 35] but fit with the result in Ref.[39], where the former didn't include the adiabatic response in the dispersion function properly.

As for the growth rate, it can be roughly formulated as

$$\gamma = \Lambda R\Omega_D k_y(k_{y,\rm max} - k_y) \tag{A17}$$

TABLE III: Parameters

Parameters	ϵ_0	τ	C_i	ρ_i	δ_b	Ω_D	κ_T	κ_n
Values	1/4	1	0.1	$2\times10^{-3/2}$	0.1	1	0.4 to 0.8	0

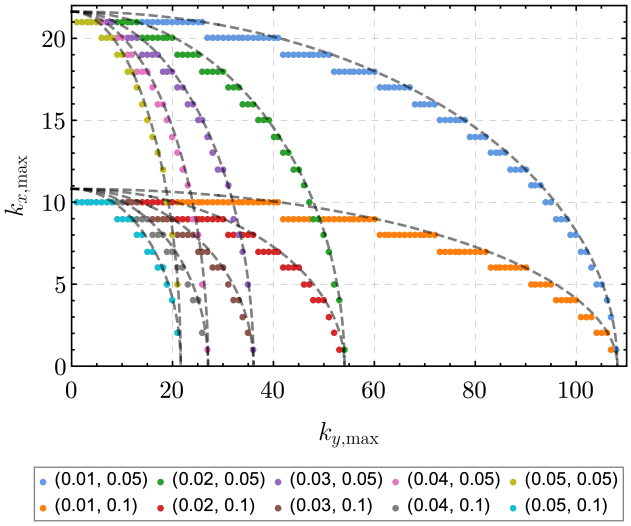

FIG. 14: $k_{x,\max}, k_{y,\max}$ for different (ρ_i, δ_b) with parameters in Table III. Data are scanned for discrete wave numbers. We can use $\rho_i^2 k_y^2 + \delta_b^2 k_r^2 = 1.17$ to fit the data points, like the dashed lines.

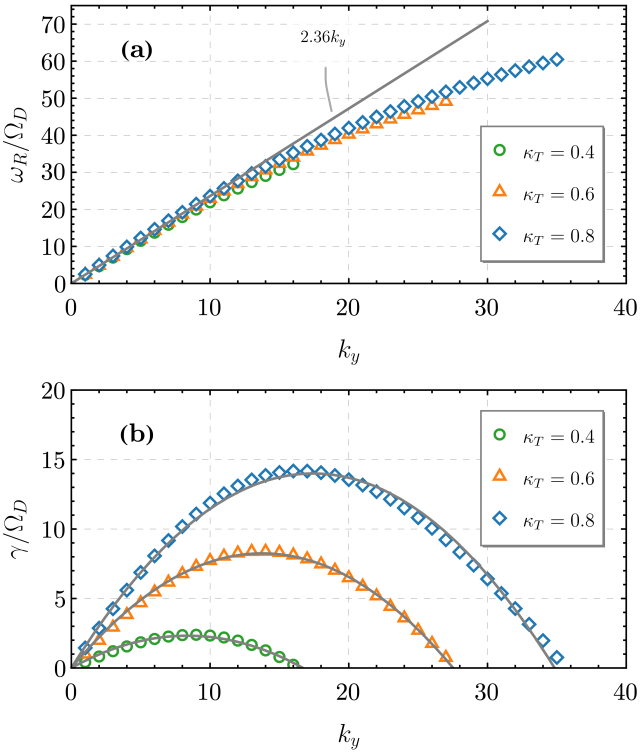

FIG. 15: Dispersion Relation, with $\delta_b^2 = 0.01, \rho_i^2 = 0.004, k_x = \pi$. (a) Real frequency in different κ_T, gray line $2.36k_y$ is an approximation. (b) Growth rate in different κ_T, gray lines are fit lines with model Eq.(A17). The resulting Λ/ρ_i are 0.223, 0.292, 0.309.

Here $k_{y,\max}$ varies with k_x and κ_T but can always be written as $k_{y,\max} = 1/(\mu_y \rho_i)$. And because of $\Theta_{\max} \lesssim 1$, there will be

$$\mu_y > 1 \tag{A18}$$

For the parameter Λ, we know it varies with k_x and κ_T. Since it has the unit of length, we can rewrite it as $\Lambda = \rho_i/\sigma$ for simplicity. From the fitting, we find that σ are always bigger than 3 in the examples in FIG. 15(b). And since Λ decreases with the increase of k_x, we have:

$$\sigma > 1 \tag{A19}$$

If we want to match the fact that when $\kappa_T < \kappa_T^c$ the growth rate will vanish, we can add a simple restriction to parameters in Eq.(A17) like below:

$$\sigma = \infty, \mu_y = \infty, \text{ when } \kappa_T < \kappa_T^c \tag{A20}$$

This leads to $\gamma = 0$ when $\kappa_T < \kappa_T^c$.

There is another useful conclusion. Using the models Eq.(A16) and Eq.(A17) above, we know the ratio between the real frequency and the growth rate is approximately:

$$\frac{\omega_R}{\gamma_{\max}} \simeq \frac{2}{\Lambda k_{y,\max}} \sim \frac{1}{\mu_y \sigma} \tag{A21}$$

Since $\mu_y \sigma > 1$, we have

$$\frac{\omega_R}{\gamma_{\max}} \sim \mathcal{O}(1) - \mathcal{O}(10) \tag{A22}$$

which is useful in the calculation of the transport coefficients in section IV C.

Appendix B: Simplification of Transport coefficients

For the flux $\langle \widetilde{T}(A - \overline{\Delta})\widetilde{V}_x \rangle$ appeared in the intensity evolution Eq.(31) in section III D, we can apply the quasi-

linear approximation:

$$\langle\widetilde{T}(A-\overline{\Delta})\widetilde{V}_x\rangle_k \sim \frac{i(A+\bar{k}_\perp^2)}{\omega-k_y\left(\Omega_Z+\frac{C_i}{\sqrt{2\varepsilon_0}}\frac{\bar{\Omega}_D}{A+\bar{k}_\perp^2}\right)} \times\langle\widetilde{V}_x^2\rangle_k\frac{1}{\sqrt{2\varepsilon_0}}\left(C_i\frac{\delta_b^2\partial_x^3\phi_Z}{A+\bar{k}_\perp^2}-\partial_x\ln\langle T\rangle\right) \tag{B1}$$

Then,

$$\langle\widetilde{T}(A-\overline{\Delta})\widetilde{V}_x\rangle \sim \chi_6\frac{C_i}{\sqrt{2\varepsilon_0}}\delta_b^2\partial_x^3\phi_Z-\chi_5\partial_x\frac{\ln\langle T\rangle}{\sqrt{2\varepsilon_0}}$$

where

$$\chi_6=\sum_k[\widetilde{V}_x(k)]^2\frac{i}{\omega-k_y\left(\Omega_Z+\frac{C_i}{\sqrt{2\varepsilon_0}}\frac{\bar{\Omega}_D}{A+\bar{k}_\perp^2}\right)}$$

$$\chi_5=\sum_k[\widetilde{V}_x(k)]^2\frac{i(A+\bar{k}_\perp^2)}{\omega-k_y\left(\Omega_Z+\frac{C_i}{\sqrt{2\varepsilon_0}}\frac{\bar{\Omega}_D}{A+\bar{k}_\perp^2}\right)}$$

All the non-resonant transport coefficients in Eq.(31)-(33) are listed as follows:

$$\chi_1^{\mathrm{n-res}}=4\int_0^{k_{y,\max}}\int_0^{k_{x,\max}}|\tilde{\phi}|^2_{k_x,k_y}\sqrt{2\varepsilon_0}(\rho_i^2k_y^2+\delta_b^2k_x^2) \times\frac{\Lambda k_y(k_{y,\max}-k_y)}{R\Omega_D\left[1+\Lambda^2\left(k_{y,\max}-k_y\right)^2\right]^2}\mathrm{d}k_x\mathrm{d}k_y \tag{B2}$$

$$\chi_2^{\mathrm{n-res}}=2\int_0^{k_{y,\max}}\int_0^{k_{x,\max}}|\tilde{\phi}|^2_{k_x,k_y}\sqrt{2\varepsilon_0}(\rho_i^2k_y^2+\delta_b^2k_x^2) \times\frac{\Lambda k_y(k_{y,\max}-k_y)}{R\Omega_D\left[1+\Lambda^2\left(k_{y,\max}-k_y\right)^2\right]}\mathrm{d}k_x\mathrm{d}k_y \tag{B3}$$

$$\chi_3^{\mathrm{n-res}}=2\int_0^{k_{y,\max}}\int_0^{k_{x,\max}}|\tilde{\phi}|^2_{k_x,k_y} \times\frac{\Lambda k_y(k_{y,\max}-k_y)}{R\Omega_D\left[1+\Lambda^2\left(k_{y,\max}-k_y\right)^2\right]}\mathrm{d}k_x\mathrm{d}k_y \tag{B4}$$

$$\chi_4^{\mathrm{n-res}}=2\int_0^{k_{y,\max}}\int_0^{k_{x,\max}}|\tilde{\phi}|^2_{k_x,k_y}\frac{1}{A+\rho_i^2k_y^2+\delta_b^2k_x^2} \times\frac{\Lambda k_y(k_{y,\max}-k_y)}{R\Omega_D\left[1+\Lambda^2\left(k_{y,\max}-k_y\right)^2\right]}\mathrm{d}k_x\mathrm{d}k_y \tag{B5}$$

$$\chi_5^{\mathrm{n-res}}=2\int_0^{k_{y,\max}}\int_0^{k_{x,\max}}|\tilde{\phi}|^2_{k_x,k_y}(A+(\rho_i^2k_y^2+\delta_b^2k_x^2)) \times\frac{\Lambda k_y(k_{y,\max}-k_y)}{R\Omega_D\left[1+\Lambda^2\left(k_{y,\max}-k_y\right)^2\right]}\mathrm{d}k_x\mathrm{d}k_y \tag{B6}$$

$$\chi_6^{\mathrm{n-res}}=\chi_3^{\mathrm{n-res}} \tag{B7}$$

Using the dispersion relation Eq.(36) and the spectrum Eq.(37), we can obtain the analytical results, for example (letting $\alpha=0$):

$$\begin{aligned}
&\chi_3^{\mathrm{n-res}}\\
&\simeq\frac{|\tilde{\phi}_0|^2}{\Omega_D}\beta\sigma\Big\{\left(\beta^2+\mu^2\sigma^2+1\right)\log\left[\left(1+\frac{1}{\beta^2}\right)\right.\\
&\quad\left.\times\left(1+\frac{1}{\mu^2\sigma^2}\right)\right]-2\cot^{-1}(\beta)\left(\beta^3-\beta\mu^2\sigma^2+\beta\right)\\
&\quad+2\mu\sigma\left(\beta^2-\mu^2\sigma^2-1\right)\cot^{-1}(\mu\sigma)\Big\}\\
&\qquad\Big/\left[\rho_i\left(\beta^2\left(2-2\mu^2\sigma^2\right)+\beta^4+\left(\mu^2\sigma^2+1\right)^2\right)\right]\\
&\sim\frac{|\tilde{\phi}_0|^2\mu^2\sigma^2}{\Omega_D\rho_i\left[\left(\mu^2\sigma^2+1+\beta^2\right)^2-4\mu^2\sigma^2\beta^2\right]}\\
&\quad\times\left[2\beta\cot^{-1}(\beta)-2\mu\sigma\cot^{-1}(\mu\sigma)\right.\\
&\qquad\left.+\log\left(\left(1+\frac{1}{\beta^2}\right)\left(1+\frac{1}{\mu^2\sigma^2}\right)\right)\right]
\end{aligned} \tag{B8}$$

where the predominate contributions are from $\mu^2\sigma^2$ related terms. Collecting those terms gives Eq.(41). For other coefficients, like $\chi_1^{\mathrm{n-res}}$, we have:

$$\chi_1^{\mathrm{n-res}}\simeq 2\sqrt{2\varepsilon_0}(\rho_i^2\langle k_y^2\rangle+\delta_b^2\langle k_x^2\rangle)\int_0^{k_{y,\max}}\int_0^{k_{x,\max}} |\tilde{\phi}|^2_{k_x,k_y}\frac{2\Lambda k_y(k_{y,\max}-k_y)}{\Omega_D\left[1+\Lambda^2\left(k_{y,\max}-k_y\right)^2\right]^2}\mathrm{d}k_x\mathrm{d}k_y \tag{B9}$$

where $\langle k_x^2\rangle$ and $\langle k_y^2\rangle$ are averaged quantities extracted from the integral. For simplicity, we just set $\langle k_x^2\rangle = Ck_{x,\max}^2$ and $\langle k_y^2\rangle = Ck_{y,\max}^2$. With the fact that we know from the dispersion relation (see Eq.(A15)):

$$\Theta_{\max}\equiv\rho_i^2k_{y,\max}^2+\delta_b^2k_{x,\max}^2\sim 1 \tag{B10}$$

where $\Theta_{\max}$ is a constant, we can write the approximation below:

$$\chi_1^{\mathrm{n-res}}=\sqrt{2\varepsilon_0}C\Theta_{\max}\chi_3^{\mathrm{n-res}} \tag{B11}$$

We can calculate all the other non-resonant transport coefficients in the same way, from $\chi_1^{\mathrm{n-res}}$ to $\chi_6^{\mathrm{n-res}}$. Let $\vartheta\equiv\sqrt{2\varepsilon_0}\Theta_{\max}C<1$ be a constant.

For resonant transport coefficient $\chi_3^{\rm res}$:

$$\chi_3^{\rm res} = \int_0^{k_{x,\max}} \int_0^{k_{y,\max}} \frac{|\tilde{\phi}_0|^2}{\pi^2 \Delta k_x \Delta k_y} \times \frac{k_y^2 \delta(\omega_R - k_y \Omega_Z - k_y b_k \bar{\Omega}_D)}{\left[1 + \left(\frac{k_x - k_{r0}}{\Delta k_x}\right)^2\right]\left[1 + \left(\frac{k_y - k_{y0}}{\Delta k_y}\right)^2\right]} \simeq \frac{|\tilde{\phi}_0|^2 k_{y,\rm res}^2 \left[|\Delta k_y \left(\Omega_Z + b_{k,\rm res}\bar{\Omega}_D\right)|\right]^{-1}}{\left[1 + \left(\frac{k_{x,\rm res}}{\Delta k_x}\right)^2\right]\left[1 + \left(\frac{k_{y,\rm res}}{\Delta k_y}\right)^2\right]} \tag{B12}$$

Put $\Theta_{\rm res}$, $\Delta k_y = \beta_y k_{y,\max} = \beta_y/(\mu_y \rho_i)$ and $\Delta k_x = \beta_x k_{x,\max} = \beta_x/(\mu_x \rho_i)$ into equation above, and set $\beta_x/\mu_x = \beta_y/\mu_y = \beta/\mu$. Then we can approximate the expression above as:

$$\chi_3^{\rm res} \simeq \frac{|\tilde{\phi}_0|^2 k_{y,\rm res}^2}{\left[1 + \left(\frac{\mu_x}{\beta_x}\right)^2 \delta_b^2 k_{x,\rm res}^2 + \left(\frac{\mu_y}{\beta_y}\right)^2 \rho_i^2 k_{y,\rm res}^2\right]} \times \frac{1}{\left|\frac{\beta_y}{\mu_y \rho_i}\left(\Omega_Z + \Omega_D \frac{3/2}{\tau + \sqrt{2\varepsilon_0}\Theta_{\rm res}}\right)\right|} \tag{B13}$$

We can set $\tau + \sqrt{2\varepsilon_0}\Theta_{\rm res} \sim 3/2$ for convenience. An approximate expression for $\chi_3^{\rm res}$ can be obtained as Eq.(B17).

Other resonant coefficients can be calculated the same way, for instance $\chi_2^{\rm res}$. Integrating the expression of $\chi_2^{\rm res}$ gives:

$$\chi_2^{\rm res} = \int_0^{k_{x,\max}} \int_0^{k_{y,\max}} \left\{ \frac{|\tilde{\phi}_0|^2}{\pi^2 \Delta k_x \Delta k_y} \times \frac{k_y^2 \delta_b(\omega_R - k_y \Omega_Z - k_y b_k \Omega_D)}{\left[1 + \left(\frac{k_x - k_{r0}}{\Delta k_x}\right)^2\right]\left[1 + \left(\frac{k_y - k_{y0}}{\Delta k_y}\right)^2\right]} \times \left(1 - \frac{1}{\tau + \sqrt{2\varepsilon_0}\left(\rho_i^2 k_y^2 + \delta_b^2 k_x^2\right)}\right) \right\} {\rm d}k_x {\rm d}k_y \simeq \frac{|\tilde{\phi}_0|^2 k_{y,\rm res}^2}{\left[1 + \left(\frac{k_{x,\rm res}}{\Delta k_x}\right)^2\right]\left[1 + \left(\frac{k_{y,\rm res}}{\Delta k_y}\right)^2\right]} \times \left(1 - \frac{1}{\tau + \sqrt{2\varepsilon_0}\left(\rho_i^2 k_{y,\rm res}^2 + \delta_b^2 k_{x,\rm res}^2\right)}\right) \times \frac{1}{|\Delta k_y \left(\Omega_Z + b_{k,\rm res}\Omega_D\right)|} \tag{B14}$$

We can approximate the expression above as:

$$\chi_2^{\rm res} \simeq |\tilde{\phi}_0|^2 k_{y,\rm res}^2 \frac{\sqrt{2\varepsilon_0}\Theta_{\rm res}}{\left[1 + \left(\frac{\mu_x}{\beta_x}\right)^2 \delta_b^2 k_{x,\rm res}^2 + \left(\frac{\mu_y}{\beta_y}\right)^2 \rho_i^2 k_{y,\rm res}^2\right]} \times \frac{1}{\left|\frac{\beta_y}{\mu_y \rho_i}\left(\Omega_Z + \Omega_D \frac{3/2}{\tau + \sqrt{2\varepsilon_0}(\delta_b^2 k_{x,\rm res}^2 + \rho_i^2 k_{y,\rm res}^2)}\right)\right|} \simeq |\tilde{\phi}_0|^2 k_{y,\rm res}^2 \frac{\beta^2 \sqrt{2\varepsilon_0}\Theta_{\rm res}}{\beta^2 + \mu^2 \Theta_{\rm res}} \frac{1}{\left|\frac{\beta_y}{\mu_y \rho_i}\left(\Omega_Z + \frac{3\Omega_D/2}{\tau + \sqrt{2\varepsilon_0}\Theta_{\rm res}}\right)\right|} \tag{B15}$$

Writing down the list of resonant transport coefficients reads:

$$\chi_2^{\rm res} = |\tilde{\phi}_0|^2 k_{y,\rm res}^2 \frac{\beta^2 \sqrt{2\varepsilon_0}\Theta_{\rm res}}{\beta^2 + \mu^2 \Theta_{\rm res}} \frac{\mu_y \rho_i}{|\beta_y \left(\Omega_Z + \Omega_D\right)|} \tag{B16}$$

$$\chi_3^{\rm res} = |\tilde{\phi}_0|^2 k_{y,\rm res}^2 \frac{\beta^2}{\beta^2 + \mu^2 \Theta_{\rm res}} \frac{\mu_y \rho_i}{|\beta_y \left(\Omega_Z + \Omega_D\right)|} \tag{B17}$$

$$\chi_4^{\rm res} = |\tilde{\phi}_0|^2 k_{y,\rm res}^2 \frac{\beta^2 (A - \sqrt{2\varepsilon_0}\Theta_{\rm res})}{\beta^2 + \mu^2 \Theta_{\rm res}} \frac{\mu_y \rho_i}{|\beta_y \left(\Omega_Z + \Omega_D\right)|} \tag{B18}$$

$$\chi_5^{\rm res} = |\tilde{\phi}_0|^2 k_{y,\rm res}^2 \frac{\beta^2 (A + \sqrt{2\varepsilon_0}\Theta_{\rm res})}{\beta^2 + \mu^2 \Theta_{\rm res}} \frac{\mu_y \rho_i}{|\beta_y \left(\Omega_Z + \Omega_D\right)|} \tag{B19}$$

Appendix C: Potential Enstrophy Budget

In this section, we discuss the potential enstrophy (PE) budget of the potential vorticity system Eq.(13)-(14) derived in section II. The potential enstrophy is defined as $\int \langle (\langle q \rangle + \delta q)^2 \rangle {\rm d}x$. First, we multiply $\langle q \rangle$ on the both sides of Eq.(13) and integrate it in x. Here we assume the domain is $x \in [L, R]$. This gives:

$$\partial_t \int_L^R \frac{1}{2} \langle q \rangle^2 {\rm d}x = - \int_L^R \partial_x \langle \widetilde{V}_x \delta q \rangle \langle q \rangle {\rm d}x \tag{C1}$$

For the fluctuation PV Eq.(14), we multiply δq on the both sides and integrate it in the whole space. This gives:

$$\partial_t \int_L^R \frac{1}{2} \langle \delta q^2 \rangle {\rm d}x + \int_L^R \left\langle \nabla \cdot \left(\tilde{V} \frac{\delta q^2}{2}\right) \right\rangle {\rm d}x = -\frac{3}{2}\Omega_D \int_L^R \langle \delta q \partial_y \widetilde{T} \rangle {\rm d}x - \langle \widetilde{V}_x \delta q \rangle \langle q \rangle \Big|_L^R + \int_L^R \partial_x \langle \widetilde{V}_x \delta q \rangle \langle q \rangle {\rm d}x \tag{C2}$$

After adding the two equations above, we see the PE budget is determined by three parts: the triplet nonlinear term, the correlation of δq and $\widetilde{T}$, and the potential vorticity flux from boundary. A quasilinear approximation

of the PV flux can be obtained using the same method in section III. So the second term in the R.H.S. of Eq.(C2) becomes:

$$\begin{aligned}\langle\widetilde{V}_x\delta q\rangle\langle q\rangle\Big|_L^R &= \chi_3 C_i\partial_x\overline{\Delta}\phi_Z\left[\frac{\ln\langle T\rangle}{\sqrt{2\varepsilon_0}}-C_i\overline{\Delta}\phi_Z\right]\Big|_L^R\\ &-(\chi_1+\chi_3)\frac{\partial_x\ln\langle T\rangle}{\sqrt{2\varepsilon_0}}\left[\frac{\ln\langle T\rangle}{\sqrt{2\varepsilon_0}}-C_i\overline{\Delta}\phi_Z\right]\Big|_L^R\end{aligned} \tag{C3}$$

If we set the boundary conditions the same as Eq.(62)-(64), then since $\partial_x\overline{\Delta}\phi_Z|_{\rm B}=0$, the first term in the R.H.S. of Eq.(C3) is 0. Finally, for the second term in the R.H.S. of Eq.(C2):

$$\begin{aligned}\langle\widetilde{V}_x\delta q\rangle\langle q\rangle\Big|_L^R &= -(\chi_1+\chi_3)\frac{\kappa_T^{\rm B}}{\sqrt{2\varepsilon_0}}\langle q\rangle\Big|_L^R\\ &\sim 2\chi^{\rm n}\frac{\kappa_T^{\rm B}}{\sqrt{2\varepsilon_0}}\langle q\rangle\Big|_L^R\end{aligned} \tag{C4}$$

where we defined $\Omega_Z=0$ at boundaries. So χ is always non-resonant at boundaries. Equation above means the constant driving heat flux from boundary times the mean PV is a source or sink for the total PE.

The first term in the R.H.S. of Eq.(C2) is actually a correlation between fluctuating temperature and vorticity, since the averaging $\langle\cdot\rangle$ is in y:

$$\begin{aligned}\int_L^R\langle\delta q\partial_y\widetilde{T}\rangle{\rm d}x &= \int_L^R\langle(\widetilde{T}-C_i\overline{\Delta}\tilde{\phi})\partial_y\widetilde{T}\rangle{\rm d}x\\ &= -C_i\int_L^R\langle\overline{\Delta}\tilde{\phi}\partial_y\widetilde{T}\rangle{\rm d}x\end{aligned} \tag{C5}$$

Here $C_i\langle\overline{\Delta}\tilde{\phi}\partial_y\widetilde{T}\rangle$ has the quasi-linear approximation:

$$\langle\overline{\Delta}\tilde{\phi}\partial_y\widetilde{T}\rangle\simeq\Theta(1-\sqrt{2\varepsilon_0}\Theta)\chi_3C_i\partial_x\overline{\Delta}\phi_Z-\Theta\chi_3\frac{\partial_x\ln\langle T\rangle}{\sqrt{2\varepsilon_0}} \tag{C6}$$

where $\Theta=\overline{\delta_b^2k_x^2+\rho_i^2k_y^2}\lesssim 1$ and $\varepsilon_0<1$, thus $\sqrt{2\varepsilon_0}\Theta<1$ and $1-\sqrt{2\varepsilon_0}\Theta\sim 1$. Putting the formula above into Eq.(C5), integrating it and assuming the system is in an initial state where $\partial_x\chi_3=0$ give the result:

$$-\frac{3}{2}\Omega_D\int_L^R\langle\delta q\partial_y\widetilde{T}\rangle{\rm d}x\simeq\frac{3}{2}\Omega_DC_i\Theta\chi^{\rm n}\langle q\rangle\Big|_L^R \tag{C7}$$

Collecting all the results above and putting them into Eq.(C2), we have the total PE budget as:

$$\partial_t\int_L^R\frac{1}{2}\left(\langle q\rangle^2+\langle\delta q^2\rangle\right){\rm d}x\simeq\left(\frac{3}{2}\Omega_DC_i\Theta-2\frac{\kappa_T^{\rm B}}{\sqrt{2\varepsilon_0}}\right)\chi^{\rm n}\langle q\rangle\Big|_L^R \tag{C8}$$

where the nonlinear term is neglected. There is a critical boundary gradient in PE budget Eq.(C8):

$$(\kappa_T^{\rm B})_C=\frac{3}{4}C_i\Omega_D\Theta\sqrt{2\varepsilon_0} \tag{C9}$$

When $\langle q\rangle|_L^R>0$ and $\kappa_T^{\rm B}>(\kappa_T^{\rm B})_C$, the total potential enstrophy of the system will decrease driving by the existing boundary heat flux. And the stronger the boundary drive is, the further the PE evolves towards reduction. Eq.(C9) has the same form as the criterion for staircase pattern triggering in Eq.(81).

REFERENCES

[1] P H Diamond, S I Itoh, K Itoh, and T S Hahm. Zonal flows in plasma - a review. *Plasma Physics and Controlled Fusion*, 47(5):R35–R161, May 2005.

[2] A Fujisawa. A review of zonal flow experiments. *Nuclear Fusion*, 49(1), January 2009.

[3] P H Diamond, S Champeaux, M Malkov, A Das, I Gruzinov, M N Rosenbluth, C Holland, B Wecht, A I Smolyakov, F L Hinton, Z Lin, and T S Hahm. Secondary instability in drift wave turbulence as a mechanism for zonal flow and avalanche formation. *Nuclear Fusion*, 41(8):1067–1080, August 2001.

[4] T S Hahm and P H Diamond. Mesoscopic transport events and the breakdown of fick's law for turbulent fluxes. *Journal of the Korean Physical Society*, 73(6):747–792, September 2018.

[5] M. J. Choi, H. Jhang, J. M. Kwon, J. Chung, M. Woo, L. Qi, S. Ko, T. S. Hahm, H. K. Park, H. S. Kim, J. Kang, J. Lee, M. Kim, and S. Y. Gunsu. Experimental observation of the non-diffusive avalanche-like electron heat transport events and their dynamical interaction with the shear flow structure. *Nuclear Fusion*, 59(8):086027, June 2019.

[6] Y Kosuga, P H Diamond, G Dif-Pradalier, and Ö D Gürcan. E×B shear pattern formation by radial propagation of heat flux waves. *Physics of Plasmas*, 21(5):055701, May 2014.

[7] G. Dif-Pradalier, G. Hornung, Ph. Ghendrih, Y. Sarazin, F. Clairet, L. Vermare, P. H. Diamond, J. Abiteboul, T. Cartier-Michaud, C. Ehrlacher, D. Esteve, X. Garbet, V. Grandgirard, O. D. Guercan, P. Hennequin, Y. Kosuga, G. Latu, P. Maget, P. Morel, C. Norscini, R. Sabot, and A. Storelli. Finding the Elusive E×B Staircase in Magnetized Plasmas. *Physical Review Letters*, 114(8), February 2015.

[8] G. Dif-Pradalier, G. Hornung, X. Garbet, Ph Ghendrih, V. Grandgirard, G. Latu, and Y. Sarazin. The E×B staircase of magnetised plasmas. *Nuclear Fusion*, 57(6):066026, April 2017.

[9] A. Ashourvan and P. H. Diamond. On the emergence of macroscopic transport barriers from staircase structures. *Physics of Plasmas*, 24(1):012305, January 2017.

[10] Weixin Guo, Patrick H Diamond, David W Hughes, Lu Wang, and Arash Ashourvan. Scale selection and feedback loops for patterns in drift wave-zonal flow turbulence. *Plasma Physics and Controlled Fusion*, 61(10):105002, October 2019.

[11] W. Wang, Y. Kishimoto, K. Imadera, J. Q. Li, and Z. X. Wang. A mechanism for the formation and sustainment of the self-organized global profile and E×B staircase in tokamak plasmas. *Nuclear Fusion*, 58(5):056005, March 2018.

[12] X. Garbet, O. Panico, R. Varennes, C. Gillot, G. Dif-Pradalier, Y. Sarazin, V Grandgirard, P. Ghendrih, and

L. Vermare. Wave trapping and E×B staircases. *Physics of Plasmas*, 28(4), April 2021.

[13] Lei Qi, M. J. Choi, Jae-Min Kwon, and T. S. Hahm. Role of zonal flow staircase in electron heat avalanches in KSTAR L-mode plasmas. *Nuclear Fusion*, 61(2), February 2021.

[14] M Leconte and T Kobayashi. Zonal profile corrugations and staircase formation: Role of the transport crossphase. *Physics of Plasmas*, page 7, January 2021.

[15] Wenbin Liu, Yihang Chen, Rui Ke, George McKee, Zheng Yan, Kairui Fang, Zengchen Yang, Zhe Gao, Yi Tan, and George R. Tynan. Evidence of $E \times B$ staircase in HL-2A L-mode tokamak discharges. *Physics of Plasmas*, 28(1):012512, January 2021.

[16] Herbert E. Huppert and J. Stewart Turner. Double-diffusive convection. *Journal of Fluid Mechanics*, 106:299–329, May 1981.

[17] N. C. Shibley and M. L. Timmermans. The formation of double-diffusive layers in a weakly turbulent environment. *Journal of Geophysical Research-Oceans*, 124(3):1445–1458, March 2019.

[18] Yana Bebieva and Mary-Louise Timmermans. Double-diffusive layering in the canada basin: An explanation of along-layer temperature and salinity gradients. *Journal of Geophysical Research-Oceans*, 124(1):723–735, January 2019.

[19] Christian Stranne, Larry Mayer, Thomas C. Weber, Barry R. Ruddick, Martin Jakobsson, Kevin Jerram, Elizabeth Weidner, Johan Nilsson, and Katarina Gardfeldt. Acoustic mapping of thermohaline staircases in the arctic ocean. *Scientific Reports*, 7, November 2017.

[20] Nicole C. Shibley, Mary-Louise Timmermans, and Christian Stranne. Analysis of acoustic observations of double-diffusive finestructure in the arctic ocean. *Geophysical Research Letters*, 47(18), September 2020.

[21] Yana Bebieva and Kevin Speer. The regulation of sea ice thickness by double-diffusive processes in the ross gyre. *Journal of Geophysical Research-Oceans*, 124(10):7068–7081, October 2019.

[22] J. S. Turner. The melting of ice in the arctic ocean: The influence of double-diffusive transport of heat from below. *Journal of Physical Oceanography*, 40(1):249–256, January 2010.

[23] Jeffrey B. Parker and John A. Krommes. Zonal flow as pattern formation. *Physics of Plasmas*, 20(10):100703, October 2013.

[24] Rameswar Singh and P H Diamond. A unified theory of zonal flow shears and density corrugations in drift wave turbulence. *Plasma Physics and Controlled Fusion*, 63(3):035015, March 2021.

[25] Prasad Perlekar, Roberto Benzi, Herman J. H. Clercx, David R. Nelson, and Federico Toschi. Spinodal Decomposition in Homogeneous and Isotropic Turbulence. *Physical Review Letters*, 112(1):014502, January 2014.

[26] Xiang Fan, P. H. Diamond, and L. Chacón. Formation and evolution of target patterns in Cahn-Hilliard flows. *Physical Review E*, 96(4):041101, October 2017.

[27] Xiang Fan, P. H. Diamond, and L. Chacón. CHNS: A case study of turbulence in elastic media. *Physics of Plasmas*, 25(5):055702, March 2018.

[28] D. G. Dritschel and M. E. McIntyre. Multiple jets as PV staircases: The Phillips effect and the resilience of eddy-transport barriers. *Journal of the Atmospheric Sciences*, 65(3):855–874, March 2008.

[29] R. M. Dorrell, J. Peakall, S. E. Darby, D. R. Parsons, J. Johnson, E. J. Sumner, R. B. Wynn, E. Ozsoy, and D. Tezcan. Self-sharpening induces jet-like structure in seafloor gravity currents. *Nature Communications*, 10, March 2019.

[30] N. J. Balmforth, S G L Smith, and W R Young. Dynamics of interfaces and layers in a stratified turbulent fluid. *Journal of Fluid Mechanics*, 355:329–358, January 1998.

[31] R V Ozmidov. On the turbulent exchange in a stably stratified ocean. *Izv. Acad. Sci. USSR, Atmos. Oceanic Phys*, 1(8):853–860, 1965.

[32] P. B. Rhines. Waves and turbulence on a beta-plane. *Journal of Fluid Mechanics*, 69(3):417–443, June 1975.

[33] Arash Ashourvan and P. H. Diamond. How mesoscopic staircases condense to macroscopic barriers in confined plasma turbulence. *Physical Review E*, 94(5):051202, November 2016.

[34] G Depret, X Garbet, P Bertrand, and A Ghizzo. Trapped ion driven turbulence in tokamak plasmas. *Plasma Physics and Controlled Fusion*, 42(9):949–971, September 2000.

[35] Y Sarazin, V Grandgirard, E Fleurence, X Garbet, Ph Ghendrih, P Bertrand, and G Depret. Kinetic features of interchange turbulence. *Plasma Physics and Controlled Fusion*, 47(10):1817–1839, October 2005.

[36] G Darmet, Ph Ghendrih, Y Sarazin, X Garbet, and V Grandgirard. Intermittency in flux driven kinetic simulations of trapped ion turbulence. *Communications in Nonlinear Science and Numerical Simulation*, 13(1):53–58, February 2008.

[37] James D Murray. *Mathematical Biology II: Spatial Models and Biomedical Applications*. Springer New York, third edition, 2001.

[38] M Tagger, G Laval, and R Pellat. Trapped ion mode driven by ion magnetic drift resonance in a fat torus. *Nuclear Fusion*, 17(1):109–113, February 1977.

[39] W M Tang, J C Adam, and David W Ross. Residual trapped-ion instabilities in tokamaks. *Physics of Fluids*, 20(3):430, March 1977.

[40] T. Cartier-Michaud, P. Ghendrih, Y. Sarazin, G. Dif-Pradalier, T. Drouot, D. Estève, X. Garbet, V. Grandgirard, G. Latu, C. Norscini, and C. Passeron. Staircase temperature profiles and plasma transport self-organisation in a minimum kinetic model of turbulence based on the trapped ion mode instability. *Journal of Physics: Conference Series*, 561:012003, November 2014.

[41] Q Yan and P H Diamond. Physics of turbulence spreading and explicit nonlocality. *Plasma Physics and Controlled Fusion*, 63(8):085017, June 2021.

[42] L Chen, Z Lin, and R White. Excitation of zonal flow by drift waves in toroidal plasmas. *Physics of Plasmas*, 7(8):3129–3132, July 2000.

[43] W Dorland and G W Hammett. Gyrofluid turbulence models with kinetic effects. *Physics of Fluids B: Plasma Physics*, 5(3):812–835, March 1993.

[44] P N Guzdar, R G Kleva, and L Chen. Shear flow generation by drift waves revisited. *Physics of Plasmas*, 8(2):459–462, February 2001.

[45] Akira Hasegawa and Kunioki Mima. Pseudo-three-dimensional turbulence in magnetized nonuniform plasma. *Physics of Fluids*, 21(1):87, January 1978.

[46] J G Charney. Geostrophic turbulence. *Journal of the atmospheric sciences*, 28(6):1087–1095, September 1971.

[47] Brian Hoskins. Potential vorticity and the PV perspec-

tive. *Advances in Atmospheric Sciences*, 32(1):2–9, January 2015.

[48] Mark P. Baldwin, Peter B. Rhines, Huei-Ping Huang, and Michael E. McIntyre. The Jet-Stream Conundrum. *Science*, 315(5811):467–468, January 2007.

[49] P S Marcus. Jupiter great red spot and other vortices. *Annual review of astronomy and astrophysics*, 31:523–573, September 1993.

[50] Akira Hasegawa and Masahiro Wakatani. Plasma Edge Turbulence. *Physical Review Letters*, 50(9):682–686, February 1983.

[51] Akira Hasegawa and Masahiro Wakatani. Self-organization of electrostatic turbulence in a cylindrical plasma. *Physical Review Letters*, 59(14):1581–1584, October 1987.

[52] Ö D. Gürcan and P. H. Diamond. Zonal flows and pattern formation. *Journal of Physics A: Mathematical and Theoretical*, 48(29):293001, July 2015.

[53] P H Diamond, S-I Itoh, and K Itoh. *Modern Plasma Physics*, volume 1. Cambridge University Press, 2010.

[54] Z Lin, S Ethier, T S Hahm, and W M Tang. Size scaling of turbulent transport in magnetically confined plasmas. *Physical Review Letters*, 88(19):195004, May 2002.

[55] R. E. Waltz and J. Candy. Heuristic theory of non-locally broken gyro-Bohm scaling. *Physics of Plasmas*, 12(7):072303, June 2005.

[56] B. F. McMillan, X. Lapillonne, S. Brunner, L. Villard, S. Jolliet, A. Bottino, T. Görler, and F. Jenko. System Size Effects on Gyrokinetic Turbulence. *Physical Review Letters*, 105(15):155001, October 2010.

[57] G Dif-Pradalier, P H Diamond, V Grandgirard, Y Sarazin, J Abiteboul, X Garbet, Ph Ghendrih, A Strugarek, S Ku, and C S Chang. On the validity of the local diffusive paradigm in turbulent plasma transport. *Physical Review E*, 82(2):025401, August 2010.

[58] Y Kosuga, P H Diamond, and Ö D Gürcan. How the propagation of heat-flux modulations triggers E×B flow pattern formation. *Physical Review Letters*, 110(10):105002, March 2013.

[59] Andrei D. Polyanin and Valentin F. Zaitsev. *Handbook of Nonlinear Partial Differential Equations*. Chapman and Hall/CRC, second edition, April 2016.

[60] M. A. Leontovich, editor. *Reviews of Plasma Physics*. Springer US, Boston, MA, 1995.

[61] J. C. Li and P. H. Diamond. Another look at zonal flows: Resonance, shearing, and frictionless saturation. *Physics of Plasmas*, 25(4):042113, April 2018.

[62] A. Di Siena, R. Bilato, T. Görler, A. Bañón Navarro, E. Poli, V. Bobkov, D. Jarema, E. Fable, C. Angioni, Ye. O. Kazakov, R. Ochoukov, P. Schneider, M. Weiland, F. Jenko, and the ASDEX Upgrade Team. New high-confinement regime with fast ions in the core of fusion plasmas. *Physical Review Letters*, 127(2):025002, July 2021.

[63] A. Di Siena, R. Bilato, T. Görler, E. Poli, A. Bañón Navarro, D. Jarema, and F. Jenko. Core transport barriers induced by fast ions in global gyrokinetic GENE simulations. *Plasma Physics and Controlled Fusion*, 64(6):064003, May 2022.